8-1-2022

Glucose Uptake by GLUT1 in Photoreceptors is Essential for Outer Segment Renewal and rod Photoreceptor Survival

Lauren L. Daniele
Thomas Jefferson University

John Y.S. Han
Thomas Jefferson University

Ivy S Samuels
Louis Stokes Cleveland VA Medical Center

Ravikiran Komirisetty
Thomas Jefferson University

Nikhil Mehta
Thomas Jefferson University

See next page for additional authors

Received: 22 March 2022 | Revised: 27 May 2022 | Accepted: 10 June 2022

DOI: 10.1096/fj.202200369R

RESEARCH ARTICLE

THE FASEB JOURNAL

Glucose uptake by GLUT1 in photoreceptors is essential for outer segment renewal and rod photoreceptor survival

Lauren L. Daniele[1] | **John Y. S. Han**[1] | **Ivy S. Samuels**[2,3] | **Ravikiran Komirisetty**[1] | **Nikhil Mehta**[1] | **Jessica L. McCord**[1] | **Minzhong Yu**[2,4] | **Yekai Wang**[5,6] | **Kathleen Boesze-Battaglia**[7] | **Brent A. Bell**[8] | **Jianhai Du**[5,6] | **Neal S. Peachey**[2,3,4] | **Nancy J. Philp**[1]

[1]Department of Pathology, Anatomy, and Cell Biology, Thomas Jefferson University, Philadelphia, Pennsylvania, USA

[2]Cole Eye Institute, Cleveland Clinic, Cleveland, Ohio, USA

[3]Louis Stokes Cleveland VA Medical Center, Cleveland, Ohio, USA

[4]Department of Ophthalmology, Cleveland Clinic Lerner College of Medicine of Case Western Reserve University, Cleveland, Ohio, USA

[5]Department of Ophthalmology and Visual Sciences, West Virginia University, Morgantown, West Virginia, USA

[6]Department of Biochemistry, West Virginia University, Morgantown, West Virginia, USA

[7]Department of Basic and Translational Sciences, Penn Dental Medicine, University of Pennsylvania, Philadelphia, Pennsylvania, USA

[8]Department of Ophthalmology, University of Pennsylvania, Philadelphia, Pennsylvania, USA

Correspondence
Nancy J. Philp, Department of Pathology, Anatomy, and Cell Biology, Thomas Jefferson University, 1020 Locust Street, Philadelphia, PA 19107, USA.
Email: nancy.philp@jefferson.edu

Funding information
HHS | NIH | National Eye Institute (NEI), Grant/Award Number: R01EY026525(NJPandKBB), R01EY12042, R01EY031324, R01EY032462 and P30EY025585; HHS | NIH | National Institute on Alcohol Abuse and Alcoholism (NIAAA), Grant/Award Number: T32AA007463(JH); Research to Prevent Blindness (NSP); U.S. Department of Veterans Affairs (VA), Grant/Award Number: I01BX002340(NSP), IK6-BX005233(ISS) and I01BX005844(NSP)

Abstract

Photoreceptors consume glucose supplied by the choriocapillaris to support phototransduction and outer segment (OS) renewal. Reduced glucose supply underlies photoreceptor cell death in inherited retinal degeneration and age-related retinal disease. We have previously shown that restricting glucose transport into the outer retina by conditional deletion of *Slc2a1* encoding GLUT1 resulted in photoreceptor loss and impaired OS renewal. However, retinal neurons, glia, and the retinal pigment epithelium play specialized, synergistic roles in metabolite supply and exchange, and the cell-specific map of glucose uptake and utilization in the retina is incomplete. In these studies, we conditionally deleted *Slc2a1* in a pan-retinal or rod-specific manner to better understand how glucose is utilized in the retina. Using non-invasive ocular imaging, electroretinography, and histochemical and biochemical analyses we show that genetic deletion of *Slc2a1* from retinal neurons and Müller glia results in reduced OS growth and progressive rod but not cone photoreceptor cell death. Rhodopsin levels were severely decreased even at postnatal day 20 when OS length was relatively normal. Arrestin levels were not

Abbreviations: cSLO, confocal scanning laser ophthalmoscopy; ERG, electroretinogram; MGC, Müller Glial Cell; MPC, mitochondrial pyruvate carrier; OS, outer segment; RPE, retinal pigment epithelium; RP, retinitis pigmentosa; SD-OCT, spectral domain optical coherence tomography.

Lauren L. Daniele, John Y. S. Han, and Ivy S. Samuels contributed equally to this work.

changed suggesting that glucose uptake is required to synthesize membrane glycoproteins. Rod-specific deletion of *Slc2a1* resulted in similar changes in OS length and rod photoreceptor cell death. These studies demonstrate that glucose is an essential carbon source for rod photoreceptor cell OS maintenance and viability.

KEYWORDS

glucose depervation, GLUT1, photoreceptors, retina, rhodopsin, *Slc2a1*

1 | INTRODUCTION

As is the case in the brain, the main energy source for the neural retina is glucose, and a decrease in glucose availability in the outer retina has been implicated in photoreceptor death in retinitis pigmentosa (RP) as well as age-related macular degeneration.[1–7] Therefore, unraveling how glucose and its metabolic derivatives support retinal health and function is essential to develop treatment strategies for retinal degenerative and age-related diseases.

Photoreceptor-specific genetic disruption of glycolytic enzymes in mice has been used to understand how aerobic glycolysis supports the metabolism and function of the mouse outer retina.[4,6,8–12] In many cases, enzyme deletion only partially disrupts the pathway of interest due to compensation by alternate pathways and isozymes.[6,9] Additionally, enzymes may have non-enzymatic functions further complicating the interpretation of the phenotype.[11,13] In contrast, targeted deletion of solute transporters themselves can provide a clearer understanding of the role(s) played by a given metabolite, such as glucose, in supporting cellular metabolism.[7,14,15]

It is well established that the retina consumes glucose for aerobic glycolysis, converting over 90% to lactate, to supply roughly half of the ATP produced.[16–19] It is hypothesized that the majority of retinal aerobic glycolysis occurs in photoreceptors.[20] However, when we restricted glucose transported to photoreceptors by knocking out the glucose transporter GLUT1, encoded by *Slc2a1*, in the retinal pigment epithelium (RPE) we did not find decreased levels of ATP in the neural retina, despite observing a decrease in levels of retinal lactate.[7] While rod photoreceptors constitute 50% of the cells in the neural retina, rod-specific knockout of lactate transporters,[14] or other enzymes required for aerobic glycolysis (HK2 and PKM2),[6,9] resulted in only ~14%–20% decrease in lactate efflux. Furthermore, mice with a conditional deletion of the mitochondrial pyruvate carrier (MPC) presented with reduced electroretinograms (ERGs) but more modest changes in photoreceptor cell number or outer segment (OS) length.[4] These studies suggest that glycolysis, the pentose phosphate shunt, and oxidative metabolism combine to support the metabolic demands of photoreceptor cells.

The daily renewal of OSs is essential for maintaining visual function in photoreceptors and requires abundant synthesis and post-translational modification of opsin. It has been clearly demonstrated that glucose and glycolysis are required to sustain OS renewal.[7,21] Glucose and its glycolytic intermediates have been found to be important precursors for protein, nucleotide, and lipid synthesis,[22] all of which are important for photoreceptor OS renewal. It was previously shown that glucose deprivation results in decreased G-protein glycosylation,[23] and that mutations of rhodopsin glycosylation sites resulted in decreased rhodopsin maturation and trafficking, shortening of OS length, and photoreceptor cell death,[24] suggesting glucose is required for the synthesis and maturation of opsin. To directly investigate how glucose is utilized in the retina, we generated and characterized mouse models lacking the glucose transporter GLUT1 in retinal neurons and Müller glia, or only in rod photoreceptors. We demonstrate that GLUT1 is the primary glucose transporter in the outer retina and that glucose deprivation leads to a reduction in rod and cone opsins and shortened OS. These studies emphasize that in addition to the catabolic metabolism of glucose to produce ATP and lactate, glucose is required for anabolic metabolism in photoreceptor cells to support OS renewal.

2 | MATERIALS AND METHODS

2.1 | Animal models

Mice carrying a floxed *Slc2a1* allele, a gift from E. Dale Abel (Jax stock #031871),[25] were crossed to two different transgenic mouse lines to target the deletion of *Slc2a1* in a pan-retinal or rod-photoreceptor-specific manner. The generation of *Crx-Cre; Glut1*$^{flox/flox}$ mice (hereafter *RetΔGlut1*) has been described[26]; control littermates were *Glut1*$^{flox/+}$*Cre*-positive and *Glut1*$^{flox/flox}$ *Cre*-negative mice. To generate a tamoxifen-inducible line lacking *Glut1* in rod photoreceptors (*Rod-Cre; Glut1*$^{flox/flox}$; hereafter *RodΔGlut1*), we crossed *Glut1*$^{flox/flox}$ mice with a transgenic line in which tamoxifen-inducible *Cre recombinase* has been knocked into the rod-specific *PDE6G* allele, a gift from Stephan Tsang.[27] Tamoxifen (100 mg/ml in ethanol, diluted with corn oil to 10 mg/ml, administered by intraperitoneal injection at 100 μg/g body weight on 3 consecutive days beginning at 5 weeks of age) was also administered to control littermates

(*Glut1*$^{flox/flox}$; *Cre negative*). All animals were kept under a 12:12 light–dark cycle. All animal procedures were conducted with the approval of the Institutional Animal Care & Use Committees of Thomas Jefferson University, the Louis Stokes Cleveland VA Medical Center, or the Cleveland Clinic, and conformed to the ARVO statement for use of animals in ophthalmic and vision research.

2.2 | Single cell RNAseq analysis

scRNAseq libraries of neural retinas from 1-month-old wild-type animals (GSE153673) were downloaded.[28] To begin, the experimental samples from methanol-fixed tissue and the NRL-GFP transgenic mouse line were excluded. The remaining four datasets (GSM4649092, GSM4649093, GSM4649095, and GSM4649096) were read into the R-studio (v2022.02.2 Build 485) using the Seurat package[29,30] function "Read10X_h5." Following the Seurat vignettes for basic scRNAseq-seq integration and "sctransform," the data were combined and normalized. Cell types of each cluster were identified using known markers,[31] and scores were given to each cell by the Seurat AddModuleScore function and averaged for all markers per cell type. Similar to a published pipeline for scRNAseq analysis of the retina,[28] the maximum module score was identified and compared to the second-highest cell type score. Cells were labeled if the maximum score was at least three times the second-highest score unless the second-highest score was zero, then an arbitrary value of 1 was needed. Ambiguously scored cells were removed. Expression values were transformed into transcript per million (TPM). Genes encoding for proteins with glucose transmembrane transport activities (GO:5355) were selected for further analysis. TPM values were averaged per cell type and, after Log2 transformation, used to generate heatmaps using "pheatmap" package. Endothelial cells were not included in the heatmap.

2.3 | In situ hybridization

Tissue samples for in situ hybridization and other assays were obtained from mice euthanized by an overdose of ketamine (>100 mg/kg) and xylazine (>10 mg/kg) followed by cervical dislocation. Enucleated eyes were immediately embedded in Neg-50™ Frozen Section Medium (Cat# 6502, Thermo Scientific) and frozen in liquid nitrogen. Blocks were then cryosectioned (8 μm) and placed on positively charged Diamond white glass microscope slides (Cat#1358W, Globe Scientific, Paramus, NJ). RNAscope was performed on fresh frozen sections using probes for *Slc2a1* and *Slc2a3* with the Manual Red Detection Kit 2.5 (Advanced Cell Diagnostics, Hayward, CA) following the manufacturer's instruction. Briefly, fresh frozen sections were fixed with ice-cold 4% PFA for 15 min at 4°C and then dehydrated in ethanol. After a hydrophobic barrier was drawn around the entire slide using an ImmEdge Hydrophobic Barrier PAP Pen (Cat# H-400, Vector Laboratories, Burlingame, CA), the sections were pre-treated with hydrogen peroxide and Protease IV for 15 min. Slides were incubated with RNAscope probes for *Slc2a1* (GLUT1) (Mm-*Slc2a1*, Cat# 458671, Advanced Cell Diagnostic, Hayward, CA) or *Slc2a3* (GLUT3) (Mm-*Slc2a3*, Cat# 451571, Advanced Cell Diagnostic, Hayward, CA), for 2 h at 40°C using HybEZ™ Hybridization System (Cat# 241000, Advanced Cell Diagnostic, Hayward, CA). Preamp steps 1–6 were performed and visualized using RNAscope 2.5 HD Manual Detection Kit Red (Cat# 322350, Advanced Cell Diagnostic, Hayward, CA). Preamp step 5 for *Slc2a1* was 20, and 30 min for *Slc2a3*. Samples were washed with PBS and stained with DAPI for 5 min. The sections were mounted using Gelvatol. The sections were imaged on Zeiss LSM780 NLO confocal microscope using the 20× objective.

2.4 | Tissue preparation and immunofluorescence

Enucleated eyes were immediately placed into 4% paraformaldehyde (PFA) (Cat# 15710, Electron Microscopy Sciences, Hatfield, PA) for 2 min. The eyes were placed onto a dish in 1× PBS, and the cornea was removed. Eyecups were placed in 1 ml of 4% PFA at room temperature on a rocker. After 2 h, the lens was removed, and the remaining eye cup was equilibrated in a stepwise manner with sucrose solutions that ranged in concentration from 5% to 30%. Globes were oriented within cryomolds in Neg-50™ Frozen Section Medium (Cat# 6502, Thermo Scientific) so that the superior/inferior axis was aligned with the sectioning plane.[32] Cryosections (8 μm thick) were collected on positively charged Diamond white glass microscope slides (Cat#1358W, Globe Scientific, Paramus, NJ) and stored at −20°C.

For immunofluorescence confocal microscopy, frozen sections were brought to room temperature and a hydrophobic barrier was drawn around the samples on the slide using a Hydrophobic Barrier PAP Pen (Cat# H-400, Vector Laboratories, Burlingame, CA). 1× PBS was used to wash away the Neg-50™ Frozen Section Medium and sections were blocked in PBS with 5% BSA and 0.1% Tween 20 (PBST) for 1 h at room temperature. Antibodies were diluted in PBST with 1% BSA and sections were incubated with the primary antibodies overnight at 4°C. The slides were washed 3x with PBST and then incubated with the appropriate Alexa Fluor 488—or Alexa Fluor 555—conjugated secondary antibodies diluted in PBST with 1% BSA for 30 min. See Table 1 for sources and dilutions of all primary and secondary antibodies used for immunofluorescence labeling. Slides were then washed 3× in PBST and 1× in PBS then

TABLE 1 Antibodies used in this study

Antigen	Supplier	Product no.	Species	Dilution (WB)	Dilution (IF)
GLUT1	Alpha Diagnostics	GT11-A	Rabbit	1:2000	1:250
GLUT3	Alpha Diagnostics	GT31-A	Rabbit	1:1000	1:100
Rhodopsin	Santa Cruz	sc-57 432 (1D4)	Mouse	1:1000	1:250
Rod arrestin (Arr1)	Philp Lab		Rabbit	1:1000	Not used
M-opsin	Millipore	ab5405	Rabbit	1:1000	1:200
Cone arrestin (Arr3)	EMD/Millipore	ab15282	Rabbit	1:1000	1:1000
Iba-1	Waco	19-19741	Rabbit	Not used	1:100
Vinculin	Cell Signaling	13901	Rabbit	1:1000	Not used
β-Actin	Cell Signaling	4970	Rabbit	1:2000	Not used
Anti-mouse IgG-488	Invitrogen	A32766	Donkey	Not used	1:500
Anti-mouse IgG-555	Invitrogen	A32773	Donkey	Not used	1:500
Anti-rabbit IgG-488	Invitrogen	A32790	Donkey	Not used	1:500
Anti-rabbit IgG-555	Invitrogen	A32794	Donkey	Not used	1:500
Anti-rabbit IgG-HRP	Jackson Immuno Research	111-035-144	Goat	1:2000	Not used
Anti-mouse IgG-HRP	Jackson Immuno Research	115-035-062	Goat	1:2000	Not used

incubated with DAPI for 10 min. Slides were washed 2× in PBS and coverslips were mounted with Gelvatol. For avidin labeling, slides were washed 3× in PBS with 0.1% Tween 20 and then incubated with avidin conjugated to Alexa Fluor 488 (Cat# A21370, Thermo Fisher Scientific) for 1 h at room temperature, followed by washes, DAPI counterstaining and mounting as above. All slides were imaged using a Zeiss LSM780 NLO confocal/multiphoton microscope.

2.5 | Western blot

Retinas were isolated from eyecups and protein was extracted using 100 µl per retina in Pierce@ RIPA buffer (Radioimmunoprecipitation Assay, Cat# 89900, Thermo Scientific, Rockford, IL) with Halt™ Protease Inhibitor (Cat# 78420, Thermo Scientific). Retinal samples were homogenized by trituration with a P200 pipette. Samples were placed on ice for 30 min with intermittent vortexing. The samples were centrifuged at 12000×RPM for 30 min, and the supernatants were removed for protein quantification by BCA Protein Assay Kit (Cat # 23225, Thermo Fisher Scientific). A total of 5, 2.5, or 0.25 µg of retina protein was loaded on 4%–12% NuPage Bis-Tris Protein gels (Cat# NP0321BOX, Invitrogen). Gels were run for 50 min at 200 V, as per the manufacturer's instructions. Gels were transferred electrophoretically onto EMD Millipore™ Immobilon™-P PVDF Transfer Membranes (Cat# IPVH00010, EMD Millipore™) at 20 V for 1 h. Membranes were incubated for 1 h at room temperature in blocking buffer (5% low-fat powdered milk in Tris-buffered saline with 0.1% Tween20 [TBST]) and incubated overnight with antibodies at 4°C in blocking buffer. See Table 1 for sources and dilutions of all primary and secondary antibodies used for western blotting. Membranes were washed 3 times with TBST and incubated for 30 min with a secondary antibody in blocking buffer at room temperature. Blots were developed using chemiluminescence (SuperSignal™ West Pico PLUS, Cat# 34577, Thermo Fisher Scientific) on FluorChem M Protein Simple detection system (San Jose, CA).

2.6 | Confocal scanning laser ophthalmoscopy (cSLO) and spectral domain optical coherence tomography (SD-OCT)

Procedures for cSLO and SD-OCT have been previously described.[14] In short, mice were anesthetized with ketamine (100 mg/kg) and xylazine (10 mg/kg), and the eyes were anesthetized with 0.5% proparacaine hydrochloride ophthalmic solution (NDC: 17478-263-12, Akorn Inc., Lake Forest, IL). Pupils were dilated with 1% tropicamide eye drops. Ocular eye shields[33,34] and Systane Ultra Lubricant Eye Drops (Alcon Laboratories, Inc., Fort Worth, TX) were used to keep eyes hydrated. The Spectralis HRA + OCT (Heidelberg Engineering, Inc., Franklin, MA) was used to obtain infrared reflectance (815 nm) and autofluorescence (excitation 486 nm/emission 500–680 nm) images of the retina using a 55° wide-field objective lens. Following cSLO, imaging of retinal lamina structure was accomplished using a Bioptigen Envisu R2210 SD-OCT system (Leica Microsystems, Buffalo Grove, IL). Image J v1.52p was used to analyze cSLO images to quantify the number of hyperfluorescent foci. SD-OCT scans were quantified manually using Bioptigen Diver version 3.4.4 (Leica Microsystems,

Buffalo Grove, IL). Animals were imaged at various time points within 1 week of indicated time points.

2.7 | Electroretinogram

Two ERG paradigms were employed as previously described.[7,14,26] For *RetΔGlut1* mice, after overnight dark adaptation, mice were anesthetized with sodium pentobarbital (65 mg/kg), the corneal surface was anesthetized (1% proparacaine HCl), and the pupils were dilated (1% tropicamide, 2.5% phenylephrine HCl, and 1% cyclopentolate). Mice were placed on a temperature-regulated heating pad throughout the recording session. ERGs were recorded in response to strobe flash stimuli presented in the dark by an Espion E3 ColorDome Full-field Ganzfeld (Diagnosys, Lowell, MA). An Ag/AgCl electrode in contact with the cornea was referenced to an Ag/AgCl pellet electrode placed in the mouth of the mouse and a ground lead was placed in the tail of the mouse.

For *RodΔGlut1* mice, animals were first dark-adapted and then anesthetized with ketamine (80 mg/kg) and xylazine (16 mg/kg). Pupils were dilated with eyedrops as described above and mice were placed on a temperature-regulated heating pad. ERGs were recorded in response to strobe flash stimuli presented in the dark by an UTAS Bigshot ERG system (LKC Technologies, Gaithersburg, MD).

For both protocols, 10 strobe stimuli ranging from −3.6 to 2.1 log candela (cd)·s/m^2 were presented in order of increasing flash strength, and the number of successive trials averaged together decreased from 20 for low-level flashes to 2 for the highest flash stimuli. The duration of the interstimulus interval increased from 4 s for low luminance flashes to 90 s for the highest stimuli. Immediately after the dark-adapted recording, a steady 20 cd/m^2 adapting field was presented in the ganzfeld bowl. After 7 min of light adaptation, photopic cone ERGs were recorded to strobe flash stimuli (−1 to 2 log cd·s/m^2) superimposed on the adapting field.

The amplitude of the a-wave was measured at a fixed time point (8.32 ms for *RetΔGlut1*; 8 ms for *RodΔGlut1*) after the flash onset from the pre-stimulus baseline. The dark-adapted b-wave amplitude was measured from the a-wave amplitude trough to the peak of the b-wave. The amplitude of the light-adapted ERG was measured from the initial negative trough to the peak of the response. For graphs presenting multiple time points, the relative scotopic a-wave, scotopic b-wave, and photopic b-wave amplitudes presented are derived from the average response to a 1.4 log cd·s/m^2 flash at each time point.

2.8 | Retinal and RPE flat mounts

Enucleated eyes were immediately placed into 4% paraformaldehyde (PFA) (Cat# 15710, Electron Microscopy Sciences, Hatfield, PA) for 8 min. For RPE flat mounts, the mice were sacrificed 2–3 h after lights went on in the animal facilities. The procedures for RPE flat mounts were performed as described.[7,14] For retinal flat mounts, the eyes were placed onto a dish in 1× PBS, and the cornea and lens were removed. Eyecups were placed back in 4% PFA for 8 min. The retinas were then carefully separated from the RPE/choroid and washed in 1× PBS. The fixed retinas were permeabilized and blocked in 5% BSA 0.1% Triton X-100 for 1 h, then incubated in primary antibody overnight in 1% BSA + 0.1% Triton X-100 at 4°C (Table 1). The retinas were washed with PBS, and secondary antibody and DAPI were applied in 1% BSA + 0.1% Triton X-100 for 1 h at room temperature. Retinas were then washed in PBS and placed on a glass slide. Retinas were then flattened with 4–6 radial cuts and slides were cover-slipped using Gelvatol.

2.9 | Image analysis and quantification

Quantification of cone arrestin positive cells was performed in Image J v1.52p[35] using the auto local threshold algorithm, followed by automated particle detection algorithms performed on thresholded images. Representative flat-mount images were taken using Zeiss LSM780 NLO confocal/multiphoton microscope. Quantification of rod and cone OS lengths was performed on images from retina cryosections immunolabeled with antibodies to rhodopsin or cone opsin. Quantification was performed using ImageJ with OS position and length information stored using the ROI manager plugin. The number of TUNEL and avidin positive nuclei were manually counted within ImageJ.

2.10 | RNA isolation, cDNA synthesis, and quantitative PCR

Neural retinas were isolated and placed immediately into 1 ml TRIzol (Cat# 15596026, Thermo Fisher Scientific), after which they were homogenized using a 1 ml syringe with an 18G needle (Cat# 305195, BD PrecisionGlide Needle), then with a 25G needle (Cat# 305124, BD PrecisionGlide Needle). RNA was extracted according to manufacturer specifications. RNA was quantified with a NanoDrop (ND-1000, Thermo Fisher Scientific). RNA (1 μg) was reverse transcribed to cDNA with a final volume of 20 μl using EcoDry Premix ([oligo dT] Cat # 639543 Takara Bio U.S.A., Mountain View, CA).

cDNA derived from 1 μg of mRNA was used for qPCR and was performed with PowerUp SYBR Green Master Mix (Cat# A25742, Thermo Fisher Scientific) on a QuantStudio 5 Real-Time PCR System (Cat# A28139, Thermo Fisher Scientific). The PCR reaction was performed according to the manufacturer's protocol. All primers (Table 2) were designed for an annealing temperature of 60°C. In short,

TABLE 2 Primers used in this study

	Forward (5′−3′)	Reverse (5′−3′)
Primers for qPCR		
Rplp0	AGATTCGGGATATGCTGTTGGC	TCGGGTCCTAGACCAGTGTTC
Rho	CCACCACCCTCTACACATCAC	ACCACAGGGCGATTTCACC
Opn1mw	TCTATGGCTACTTCGTTCTGGG	GCCTGTGATTCCACACAATGA
Arrestin 1 (Arr1)	GGTCAGGGTGACATACACCTT	GCCTGCGGGAAGACCAATAAA
Arrestin 3 (Arr3)	GAGCCCATTGATGGAGTCGT	GGGCAGGTTAGCAACCATCT
Primers for genotyping		
GLUT1 flox	CTGTGAGTTCCTGAGACCCTG	CCCAGGCAAGGAAGTAGTTC
Cre	CCATCTGCCACCAGCCAG	TCGCCATCTTCCAGCAGG
Pde6g$^{tm1(CRE/ERT2)}$	GGTCAGATTCCAGTGTGTGGG	CTTAGGTGGTCCTTTCCTGGG
		GTTTAGCTGGCCCAAATGTTG

reactions were heated to 50°C for 2 min and held to 95°C for 10 min. Samples were then denatured at 95°C. Cycle threshold (Ct) values were generated by the software and normalized to RPLP0. Values of $2^{-(\Delta\Delta Ct)}$ were used to compare levels of gene expression across animals.

2.11 | TUNEL assay

Cryosections from 4% PFA fixed eyes were used for the detection of apoptotic cells with ApopTag® Fluorescein In Situ Apoptosis Detection Kit (Millipore, Cat# S7110), following manufacturer instructions. In short, frozen sections were brought to room temperature, and a hydrophobic barrier was drawn around the entire slide using an ImmEdge Hydrophobic Barrier PAP Pen. The sections were post-fixed in an ethanol: acetic acid solution for 5 min at −20°C, then washed in PBS. Equilibration buffer was applied for 1 min and aspirated. TdT enzyme was added, and sections were incubated in a HybEZ™ II Hybridization oven for 60 min at 37°C. Stop/Wash buffer was used, and the anti-digoxigenin conjugate was applied for 30 min at room temperature. Slides were then washed and counterstained with DAPI and coverslips mounted with Gelvatol. Slides were imaged using a Zeiss LSM780 NLO confocal/multiphoton microscope.

2.12 | Measurement of lactate

All steps of the assay were performed in Krebs-Ringer-Bicarbonate (KRB). KRB consisted of 98.5 mM NaCl, 4.9 mM KCl, 1.2 mM KH_2PO_4, 1.2 mM $MgSO_4$-$7H_2O$, 20 mM HEPES, 2.6 mM CaCl-$2H_2O$, and 25.9 mM $NaHCO_3$, dissolved in deionized H_2O, which was bubbled with 5% CO_2 to adjust the pH to 7.4 and filtered through a 0.22 µm membrane. Glucose was diluted with KRB solution to 5 mM (GKRB), aliquoted into 48 well plates (Cat#3548, Corning), and placed into a cell incubator at 37°C, 5% CO_2, prior to dissection. Each retina was dissected and placed in a single well of a 48-well plate in GKRB. Samples were taken after 15, 30, and 60 min and lactate in the GKRB was measured using Lactate Reagent (Cat#735-10, Trinity Biotech, Bray, Co Wicklow, Ireland).

2.13 | Metabolomics analysis

Animals were dark-adapted for 2–3 h and all procedures were performed in dim red light. Eyes were placed in ice-cold 1× Hank's Balanced Salt Solution (Cat# 88284, Thermo Fisher Scientific) over parafilm layers. The anterior segment including the lens was quickly removed and the retina was separated from the eyecup with fine forceps and flash frozen. Retinal metabolites were extracted and analyzed by targeted metabolomics using liquid chromatography with tandem mass spectrometry (LC MS/MS) as reported.[4,36] The peaks were integrated using multiquanta 3.0.2 software (Ab Sciex) and the peak intensities were imported into R-studio v2022.02.0 Build 443, using MetaboAnalyst package v3.2.0.[37] All metabolite levels were scaled by Pareto scaling, and *p*-values were obtained by *t*-test within the package.

2.14 | Statistical analysis

All graphs and statistical analysis were done using GraphPad Prism version 9.3.0 (GraphPad, San Diego, CA). Unpaired two-tailed Student's *t*-tests were performed between samples to determine the *p*-values. One-way ANOVA was performed when comparing more than two genotypes, and two-way ANOVA was performed when comparing more than two different variables. A value of $p \leq .05$ was considered significant, and represented as $p \leq .05$ (*), $p \leq .01$ (**), $p \leq .001$ (***), $p \leq .0001$ (****). All ERG data are graphed as mean ± SEM $N \geq 3$, and all other data were graphed as mean ± SD $N \geq 3$.

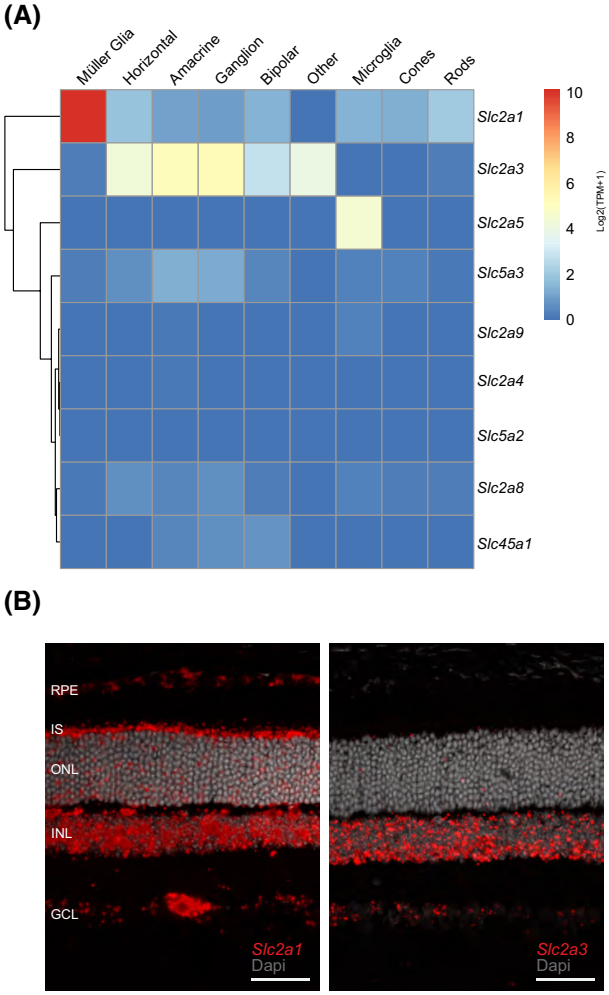

FIGURE 1 GLUT1 is the primary glucose transporter in the outer retina (A) scRNAseq analysis of genes encoding solute transporters with glucose transport activity (GO:5355) from the 1-month-old murine retina (GSE153674). Each cell type shows the Log 2 transformed average transcript per million (TPM). (B) Expression of *Slc2a1* and *Slc2a3* in control mouse retinas using in situ hybridization. The left panel shows *Slc2a1* transcript, the right panel shows *Slc2a3* transcript detected (red) (Scale bar indicates 50 μm).

3 | RESULTS

3.1 | GLUT1 and GLUT3 are the primary glucose transporters in the neural retina

Glucose is the primary metabolic substrate of the neural retina and is transported across the inner and outer blood-retinal barrier by GLUT1. The RPE forms the outer blood-retinal barrier and transports ~60%–70% of the glucose entering the retina, where it can be utilized for anabolic and catabolic metabolism.[1,7] To better understand the expression levels and cell specificity of the different glucose transporters in the retina, we analyzed scRNAseq libraries from a 1-month-old mouse neural retina (GSE153673)[28] for genes that encode proteins with glucose transmembrane transport activities (GO:5355). We found that *Slc2a1* (encoding GLUT1) and *Slc2a3* (encoding GLUT3) had the highest expression in the retina (Figure 1A). While *Slc2a1* was expressed in all retinal cells analyzed, its expression was the highest in Müller glial cells (MGCs). Furthermore, *Slc2a1* was the only transporter with high expression in rods, cones, and MGCs. In contrast, *Slc2a3* is expressed robustly in horizontal cells, amacrine cells, bipolar cells, and ganglion cells, but the expression is low in MGCs or photoreceptors. To validate the RNAseq analysis for *Slc2a1* and *Slc2a3*, we performed in situ hybridization on frozen sections of 1-month-old control retinas. The *Slc2a1* RNAscope probe labeled the RPE, inner segment layer (IS), outer nuclear layer (ONL), inner nuclear layer (INL), and the ganglion cell layer (GCL). In contrast, the *Slc2a3* RNAscope probe was primarily detected in the INL, and GCL (Figure 1B) consistent with previous reports.[38,39] Multiple cell types reside in the GCL apart from ganglion cells (including displaced amacrine cells, astrocytes, and MGC end-feet) all of which could express *Slc2a3*. Taken together our data show that GLUT1 is the major glucose transporter of the outer retina.

3.2 | Expression of *Slc2a3* does not compensate for the loss of *Slc2a1* in the outer retina of *RetΔGlut1* mice

To investigate whether GLUT1 expression in the neural retina supports visual function, we characterized transgenic mice with a pan-retinal knockout of *Slc2a1* (*RetΔGlut1*), generated by crossing the *Glut1*$^{flox/flox}$ mouse to *Crx-Cre* transgenic mice.[26,40] To confirm the excision of the *Slc2a1* gene in *RetΔGlut1* mice, we examined the expression of *Slc2a1* by in situ hybridization in the retinas of 1-month-old mice. In control mice, *Slc2a1* was detected in the inner retinal blood vessels, IS, ONL, INL, and GCL (Figure 2A, left panel) as previously shown (Figure 1B). In the *RetΔGlut1* retina, the signal was lost from the IS, ONL, INL, and GCL, but *Slc2a1* was still detected in inner retina blood vessels (arrows in Figure 2A, right panel). Sporadic *Slc2a1* signal was seen in the ONL, most likely due to mosaic expression of *Cre*.[40]

Localization of GLUT1 protein was examined by immunolabeling retinal cryosections from control and *RetΔGlut1* mice (Figure 2B). In control mice, the brightest labeling was observed in the basolateral and apical membranes of the RPE, retinal capillaries, and MGC somas and their processes in the INL and ONL (Figure 2B) as described previously.[7,26,41,42] Faint GLUT1 labeling was also detected in the IS, consistent with its distribution in photoreceptors.[7,26,41] In comparison, GLUT1 immunolabeling was mostly absent

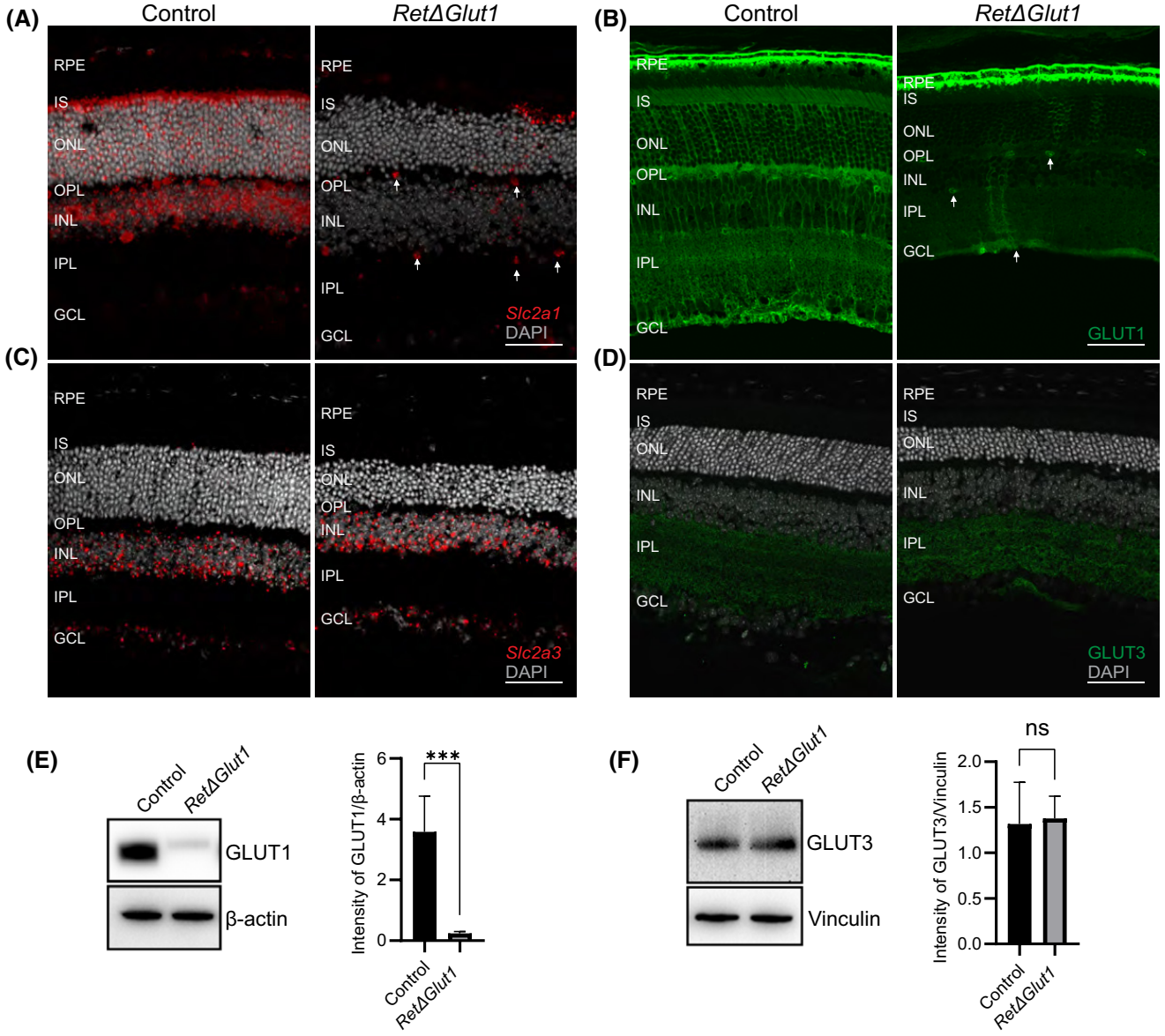

FIGURE 2 Deletion of GLUT1 from the retina does not result in compensatory changes in expression of GLUT3 (A) In situ hybridization to detect the localization of *Slc2a1*. The *RetΔGlut1* mice had a loss of *Slc2a1* (red) signal in the inner and outer retina with intermittent expression. *Slc2a1* expression is seen in inner retinal blood vessels (as indicated by white arrows) and the RPE (Scale bar indicates 50 μm). (B) Immunostaining of GLUT1 (green) in control and *RetΔGlut1* mice. White arrows indicate GLUT1 expression in inner retinal blood vessels. (Scale bar indicates 50 μm). (C) In situ hybridization of *Slc2a3* from control and *RetΔGlut1* mice at 1 month of age. (Scale bar indicates 50 μm). (D) Immunostaining of GLUT3 (green) in control and *RetΔGlut1* mice at 1 month of age. (Scale bar indicates 50 μm). (E) Western blot analysis of GLUT1 expression in control and *RetΔGlut1* retinas. 5 μg retina protein was loaded per well. Blots are representative of $N = 5$. Bars indicate the average ± SD of GLUT1 intensity normalized to β-Actin for $N = 5$ mice. (F) Western blot analysis of GLUT3 expression in control and *RetΔGlut1* retinas. 5 μg retina protein was loaded per well. Blots are representative of $N = 3$. Bars indicate the average ± SD of GLUT3 intensity normalized to Vinculin for $N = 3$ mice.

from the retinal layers of *RetΔGlut1* mice but was detected in the RPE and inner blood vessels. Consistent with the in situ data, GLUT1 staining was detected only sporadically in MGCs or photoreceptors in the outer retina.

To determine whether *Slc2a3* was increased to compensate for the loss of *Slc2a1* we performed in situ analysis with probes for *Slc2a3*. In the *RetΔGlut1*, the expression pattern was similar to that of control with most of the signal restricted to the INL and GCL along with a small scattering of signal in the ONL (Figure 2C). Immunolabeling of retina cryosections was performed to confirm that expression of GLUT3 was not altered in *RetΔGlut1* mice. In the control retinas, the highest GLUT3 expression was restricted to two bands within the IPL (Figure 2D). Previous studies have shown GLUT3 to colocalize mainly to two bands within the IPL that were identified as amacrine cells based on

their immunolabeling for choline acetyltransferase.[38,39] In *RetΔGlut1* mice, the pattern of staining for GLUT3 did not change (Figure 2D right panel). Loss of GLUT1 expression from P20 *RetΔGlut1* retinas was confirmed by immunoblot analysis of the whole retina (Figure 2E). Additionally, immunoblot analysis confirmed that GLUT3 expression levels are not altered in the retinas of *RetΔGlut1* mice (Figure 2F). Taken together these results show that GLUT1 is the primary facilitative glucose transporter in the outer retina, while GLUT3 expression is restricted to the inner retina. Our results confirm the ablation of GLUT1 expression in the *RetΔGlut1* retina and indicate that GLUT3 does not compensate for the loss of GLUT1 in the outer retina.

3.3 | Photoreceptor degeneration in *RetΔGlut1* mice

As *Crx Cre* is expressed throughout the neural retina,[40] the loss of glucose uptake may have a global impact on the neural retina. We used SD-OCT to monitor longitudinal changes in the retina between P20 and 4 months of age. Representative B-scans from the horizontal meridian are shown for 2-month-old control and 1-, 2-, and 4-month-old *RetΔGlut1* eyes (Figure 3A). Progressive thinning of the ONL was apparent in *RetΔGlut1* mice from 1 to 4 months. The *RetΔGlut1* photoreceptor lamina was also observed to have lower bright/dark signal contrast than controls indicating less signal/back-reflection from locations corresponding to the outer limiting membrane (OLM), IS/OS transition zone, and photoreceptor OS apical tips (Figure 3A). To track the progression of ONL layer changes, the ONL thickness was quantified from control and *RetΔGlut1* mice from P20 to 4 months of age (Figure 3B). The *RetΔGlut1* ONL was reduced by ~18% of control at 1 month and by 45% of control at 4 months of age (Figure 3B). In contrast, the inner retinal layer thickness measured from the OPL to the innermost GCL reflectance signal was not different in *RetΔGlut1* at any age (Figure 3C).

3.4 | *RetΔGlut1* mice have impaired visual function

The impact of GLUT1 deletion on retinal function was investigated using ERG analysis. Dark-adapted (rod photoreceptor driven) a-wave amplitudes were reduced in 1-month-old *RetΔGlut1* mice (Figure 3D). We next compared amplitudes for responses to stimuli that elicited a near-maximal response in controls and *RetΔGlut1* at different ages. At P20, near the time of first eye-opening, the response amplitude was not altered in *RetΔGlut1* mice. At 1 month of age, however, a-waves were ~25% of control ($132\,\mu V \pm 16$ vs. $508\,\mu V \pm 30$, mean ± SD).[26] Between 2 and 4 months, a-wave amplitudes were reduced further to <20% of control (Figure 3E). Dark-adapted b-waves were reduced in a similar manner, likely due to the much-diminished photoreceptor activation of bipolar neurons.

We next examined the thickness of the OS layer in B-scans as photoreceptor OS maintenance has been shown to depend on glycolytic pathways.[8,12,21] In control mice, the OS layer thickness increased from P20 to 1 month and was then maintained at ~25 μm throughout adulthood. In contrast, *RetΔGlut1* OS thickness was ~15% less than controls at P20 and failed to further increase in length during late post-natal development (Figure 3F). Our data suggest that glucose uptake via GLUT1 is necessary for the normal elaboration and maintenance of the photoreceptor OS.

Previous studies have shown that cones are less dependent on glycolysis than rods in non-degenerating retinas.[6,14,43] However, in models of RP, cones maintain their viability by upregulating aerobic glycolysis through stabilization of GLUT1 expression at the plasma membrane of cone photoreceptors.[2,6] Given that cones represent only 3% of photoreceptors in the mouse retina, it is difficult to assess impacts on cone viability with SD-OCT. To examine if loss of cone photoreceptors contributed to the observed thinning of the *RetΔGlut1* ONL, 4-month-old retinal flat mounts were immunolabeled for cone arrestin (ARR3) to quantify cone density (Figure 4A). Surprisingly, there was no difference in cone density in retinas between 4-month-old control and *RetΔGlut1* mice (Figure 4A right panel). To investigate the impact of GLUT1 loss on cone function, cone-driven responses were isolated by superimposing stimulus flashes on a rod-desensitizing background (Figure 4B). Photopic (cone-driven) b waves were reduced in *RetΔGlut1* mice at 1 month but less so compared to the dark-adapted responses. Maximum cone-driven response amplitudes were not different at P20 but were reduced to 62% of control at 1 month of age and 46% of control at 4 months (Figure 4C). The data suggest that cones of *RetΔGlut1* mice do not die although cone visual function is impaired with loss of GLUT1.

3.5 | *RetΔGlut1* mice have arrested OS development

The ERG deficits observed in *RetΔGlut1* mice were more severe than predicted by photoreceptor loss alone (Figure 3B,D). For example, at 1 month of age, ONL thickness was reduced by 18% while the maximal a-wave responses were reduced by ~75%. Furthermore, while the number of cones did not change (Figure 4A), photopic b-wave responses were reduced by ~40% (Figure 4B,C). Measurements from SD-OCT suggested that OS lengths were shorter (Figure 3F). Since

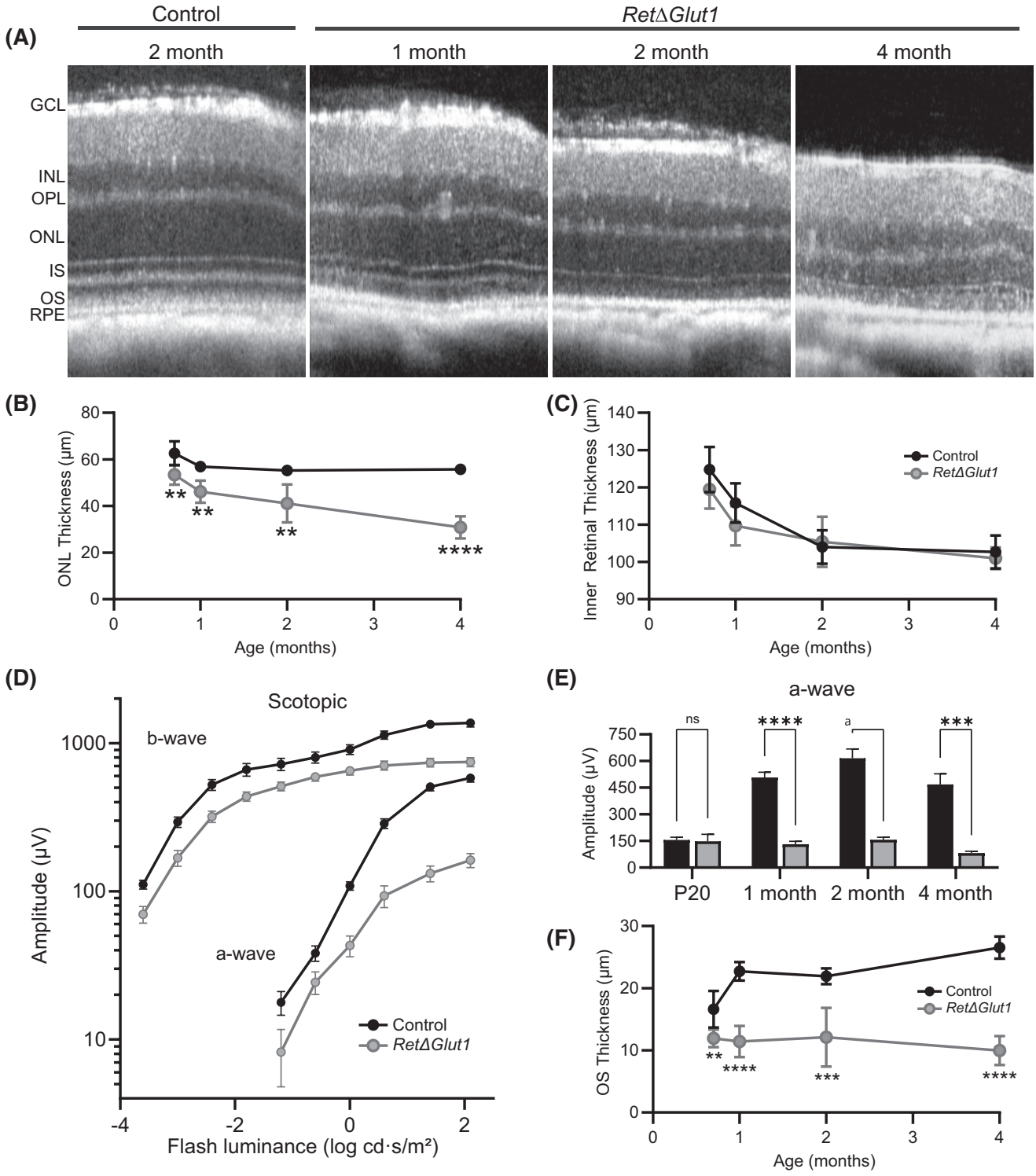

FIGURE 3 Rods degenerate in mice lacking retinal GLUT1 expression (A) Averaged SD-OCT B-scan from the horizontal meridian of retinas from 2-month-old control and 1, 2, and 4-month-old *RetΔGlut1* mice. GCL, INL, OPL, ONL, IS, OS, and RPE are indicated. (B) ONL layer thickness was measured from volumetric SD-OCT scans at P20, 1, 2, and 4 months of age. Data points indicate average (±SD) for 3–6 mice. (C) Inner Retinal Thickness (OPL-GCL) was measured from volumetric SD-OCT scans at P20, 1, 2, and 4 months of age. Data points indicate average (±SD) for 3–6 mice. (D) Luminance-response functions for a-waves and b-waves were recorded from 1-month mice. Data points indicate average (±SEM) for 13–14 mice. (E) Maximum amplitudes for a-waves (at 1.4 log cd · s/m^2 luminance) at the ages indicated. Bars indicate the average (±SEM) for 8–14 mice. (F) OS length was measured from volumetric SD-OCT scans at P20, 1, 2, and 4 months of age. Data points indicate average (±SD) for 3–6 mice.

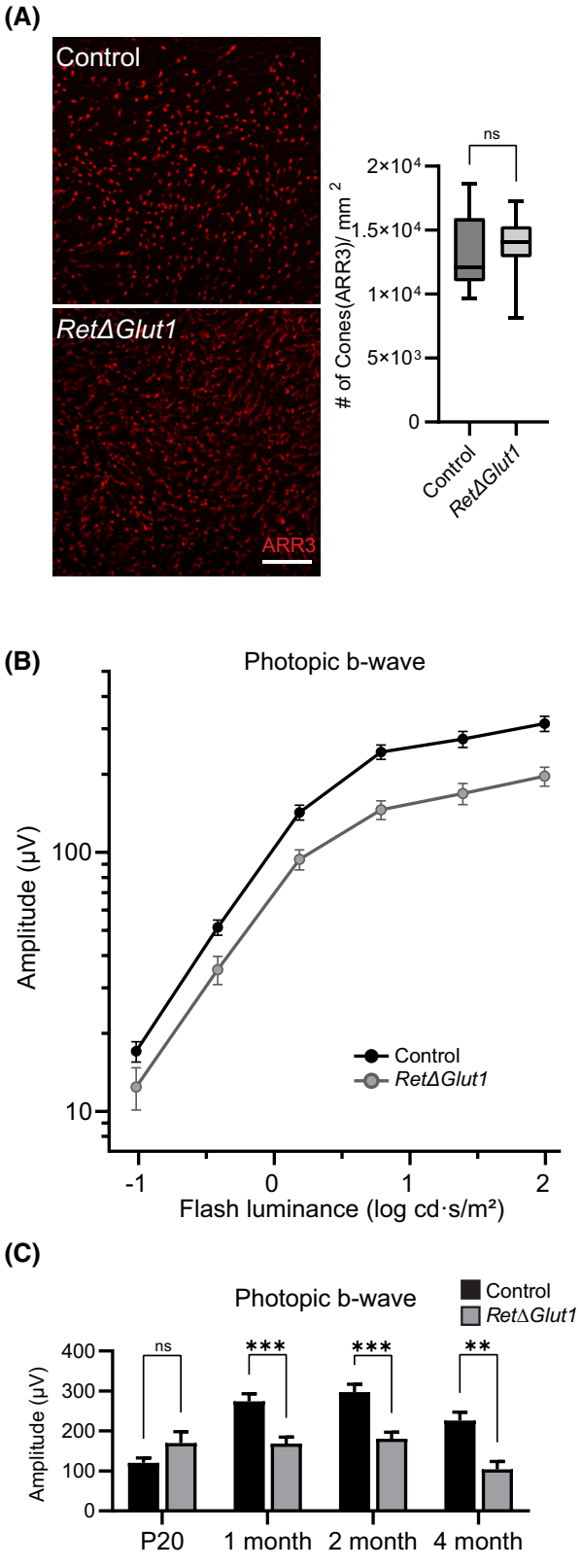

FIGURE 4 Cones of *RetΔGlut1* mice have impaired function but do not degenerate (A) Fluorescence images of retinal flat mounts immunolabeled for cone arrestin ARR3 (red). The scale bar indicates 100 μm. Box plots of estimations of cone density per mm^2 at various radial positions halfway between optic nerve and edge of the retina in flattened retinas for 3 mice. (B) Luminance response functions from photopic ERG b-waves were recorded from 1-month control and *RetΔGlut1* mice under light-adapted conditions. Data points indicate average (±SEM) for 13–14 mice. (C) Maximum amplitudes for photopic b-waves (for flashes at 1.4 log cd · s/m^2 luminance) for mice at the ages indicated. Bars indicate an average (±SEM) for 8–14 mice.

OS measurements from OCT are sensitive to fluid levels and cone OSs cannot be measured by OCT, immunolabeled cryosections were used to quantify the lengths of rod and cone OSs and examine the localization of opsin.

We quantified the OS length of rods and cones by staining, respectively, for rhodopsin (RHO) and mid-wave cone opsin (M-opsin) at P12, when the highly organized disc architecture of the OS begins to take shape[44–46] and at P30 when OSs have assumed their adult length and structure, (Figure 5A,B). RHO was localized to the OS in both control and *RetΔGlut1* mouse at both ages (Figure 5A). At P12, rod OS lengths were not significantly different between control and *RetΔGlut1* mice, indicating that initial OS formation is not impacted by lack of GLUT1 (Figure 5A). By P30, however, *RetΔGlut1* rod OSs were ~50% shorter than those of controls (Figure 5A), in agreement with our SD-OCT results (Figure 3F) and suggesting that rod OS formation is slowed in the absence of GLUT1. Similarly, M-opsin was localized to the OS in both control and *RetΔGlut1* mice at both P12 and P30 (Figure 5B) and cone OS length was not significantly different at P12, although fewer M-opsin positive cones were seen at P12, despite controlling for orientation of cryosections. At P30, although we no longer observed a decreased density of cones in the *RetΔGlut1* retina, the length of their OS was only ~50% of control. These data indicate that the rate of nascent cone OS formation may be slowed in the absence of GLUT1 such that they never achieve a fully formed OS at any age.

Opsin protein biosynthesis is a driver of OS formation, and disc morphogenesis is disrupted in photoreceptors with low opsin levels.[47–49] Intermediates of glucose metabolism serve as precursors for the synthesis of nucleotides, amino acids and glycans, and anabolic impairments in OS renewal were observed in models with disrupted glycolytic enzymes.[8,9,12,21,50] Therefore, we tested whether shortened OSs resulted from impaired protein biosynthesis in *RetΔGlut1* mice. Total levels of RHO were examined at P12, P20, and P30 (Figure 5C). These ages were chosen to correspond to eye-opening (P12), partial elaboration of the OS (P20), and the presence of a mature OS with adult RHO concentration (P30) in wild-type mice.[51,52] Retinal lysates from control and *RetΔGlut1* were run on polyacrylamide gels and blotted for GLUT1, RHO, and Rod arrestin (ARR1) (Figure 5C). While RHO levels were clearly reduced, ARR1 levels were similar between controls and

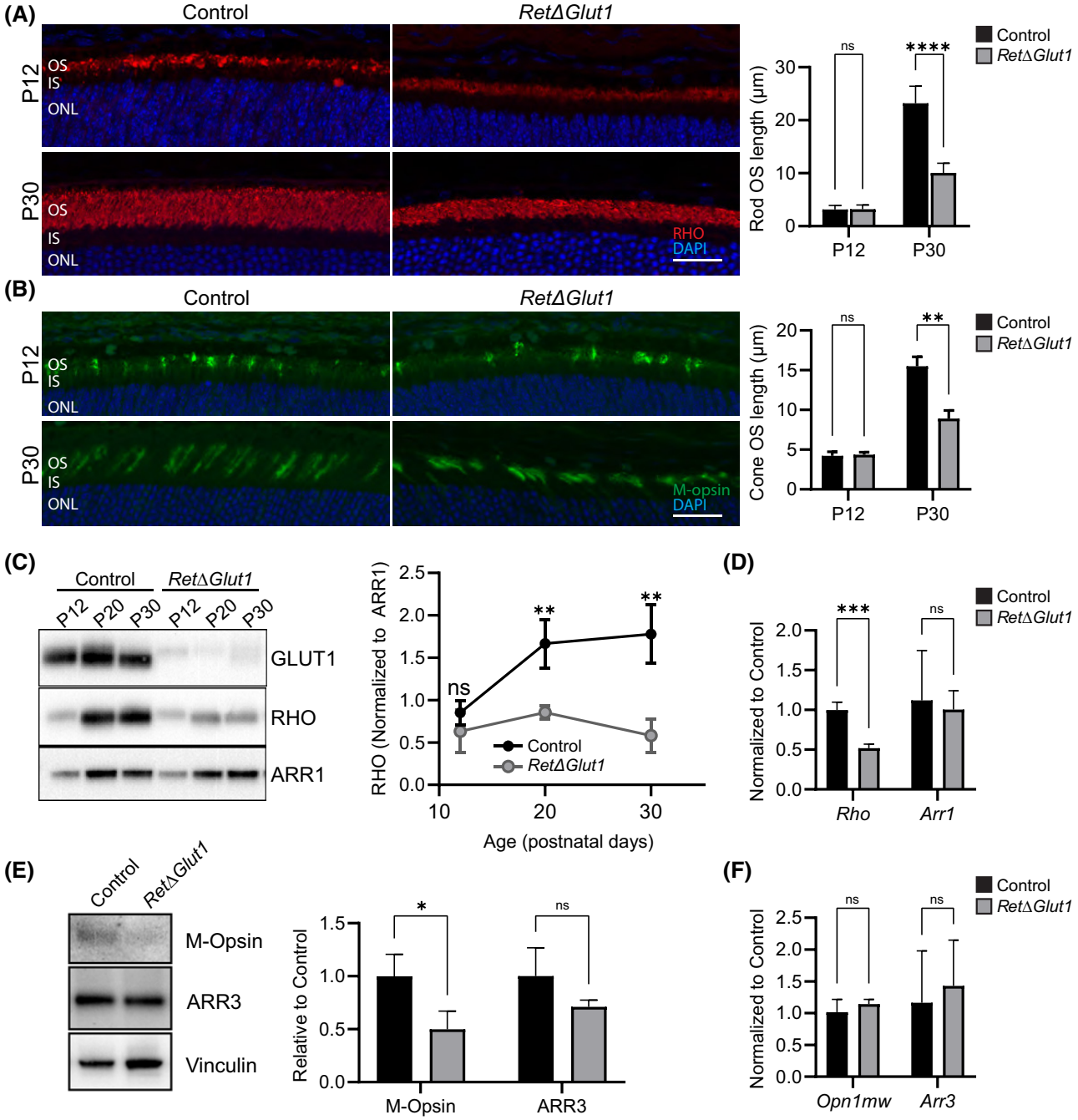

FIGURE 5 Reduced opsin synthesis contributes to the impaired renewal of rod and cone OS (A) Left: Retina cryosections from control and *RetΔGlut1* mice immunolabeled for RHO (red) and counterstained with DAPI (blue) at P12 (top row) and P30 (bottom row). OS lengths were estimated with ImageJ from images of cryosections like those shown from P12 and 1-month control and *RetΔGlut1* mice. Right: Bars indicate the average ± SD for 3 mice. Scale bar indicates 50 μm. (B) Left: Retina cryosections from control and *RetΔGlut1* mice immunolabeled for cone opsin (green) and counterstained with DAPI (blue) at P12 (top row) and P30 (bottom row). OS lengths were estimated with ImageJ from images like those shown at left, from P12 and 1-month control and *RetΔGlut1* mice. Right: Bars indicate the average ± SD for 3 mice. The scale bar indicates 50 μm. (C) Western blots showing relative GLUT1 (5 μg/well), Rhodopsin (RHO) (0.25 μg/well), and rod arrestin (ARR1) (0.25 μg/well) levels in retina lysates from control and *RetΔGlut1* mice aged P12, P20, and P30. The ratio of density signals for rhodopsin relative to ARR1 at various ages was estimated from the retinas of control and *RetΔGlut1* mice. Data points indicate average ± SD for 3 mice. (D) Relative transcription levels for rhodopsin (*Rho*) and rod arrestin (*Arr1*) estimated from real-time RT-PCR analysis with probes for mouse, *rho*, and *Arr1* for retinas of P30 control and *RetΔGlut1* mice. Bars indicate the average ± SD for 3 mice. (E) Left: Western blots showing relative M-opsin and cone arrestin (ARR3) levels in retina lysates (2.5 μg/well) from control and *RetΔGlut1* mice aged P30. Right: Ratio of density signals for M-opsin and ARR3 relative to vinculin at P30 estimated from retinas of control and *RetΔGlut1* mice. Bars indicate the average ± SD for 3 mice. (F) Relative transcription levels for M-opsin and cone arrestin estimated from real-time RT-PCR analysis with probes for mouse *Opn1mw* and (*Arr3)* for retinas of P30 control and *RetΔGlut1* mice. Bars indicate the average ± SD for 3 mice.

RetΔGlut1 at all ages examined (averaging 92%–96% of controls). Since there was no difference in ARR1 levels between controls and *RetΔGlut1* mice, we examined how the absence of retinal GLUT1 impacted the ratio of RHO to rod arrestin (RHO/ARR1) (Figure 5C). At P12 there was no difference in the RHO/ARR1 ratio between control and *RetΔGlut1* mice. However, by P20, RHO/ARR was decreased in the *RetΔGlut1* retina to ~50% of control (0.85 ± 0.08 vs. 1.67 ± 0.29) and further decreased to 33% of control (0.58 ± 0.2 vs. 1.78 ± 0.35) at P30 (Figure 5C). These data indicate that in the absence of GLUT1 and low glucose availability, the synthesis of membrane glycoproteins (RHO) is reduced more than the synthesis of cytoplasmic proteins.

We next tested the possibility that lower levels of RHO at 1 month of age were the result of reduced transcription. Our qPCR data showed that transcription of *Rho* but not *Arr1* was reduced by ~50% in *RetΔGlut1* (Figure 5D). Thus, reduced RHO results in part from the reduced transcription of *Rho*. However, we observed normal levels of ARR1 protein and *Arr1* transcript.

We next examined whether cones have similar anabolic impairments as rods of *RetΔGlut1 mice* by measuring the relative expression of M-opsin at P30 (Figure 5E). M-opsin levels of 1-month-old *RetΔGlut1* mice were 50% of controls (Figure 5E) while there was no difference in the expression of M-Opsin mRNA, encoded by the *Opn1mw gene*, between control and *RetΔGlut1* mice (Figure 5F). Moreover, expression levels of cone arrestin, (ARR3), encoded by *Arr3*, were not significantly decreased in the *RetΔGlut1* retina. Our data show that in the absence of GLUT1, transcription of *Rho* but not *Opn1mw* is impaired and that the expression of both proteins is dependent on glucose uptake.

If biosynthetic pathways for OS constituents were slowed during synthesis or maturation, due to limited availability of anabolic building blocks, we might expect increased localization of opsins in non-OS compartments. We examined the localization of rhodopsin and cone opsins by adjusting the display gain equivalently across images to amplify the signal from non-OS photoreceptor regions. We noted increased immunolabeling for rhodopsin and cone opsin in photoreceptors of *RetΔGlut1* but not in control mice (Figure S1A,B), suggesting that sluggish biosynthesis of glycoproteins in the absence of GLUT1 results in aberrant localization of opsin to non-OS compartments.

The shortened OS length suggests that OS renewal is impaired in *RetΔGlut1* photoreceptors due to anabolic deficits. However, there is a possibility that engulfment and phagocytosis of OS tips by the RPE are also disrupted in *RetΔGlut1* mice. We investigated the possibility of altered uptake of OS discs in *RetΔGlut1* mice by immunolabeling RPE flat mounts for RHO and ZO1, an RPE tight junction-specific marker. The RPE was isolated at 2.5 h after lights on, corresponding to the diurnal peak in the number of internalized phagocytosed OS in the RPE.[53] We find numerous rhodopsin-positive inclusions in the RPE from P20 and P30 *RetΔGlut1* with comparable densities to that of control RPE (Figure S2), suggesting that phagocytosis of OS by the RPE is normal.

3.6 | Inflammation accompanies photoreceptor degeneration in *RetΔGlut1* mice

Photoreceptor degeneration is frequently accompanied by microglia activation and immune cell infiltration into the subretinal space.[54,55] To examine the involvement of inflammation and its temporal relationships to cell degeneration and loss, we used cSLO with blue light stimulation to capture autofluorescence (BAF) in *en face* scans of *RetΔGlut1* and control retinas (Figure 6A). BAF scans revealed hyperfluorescent foci (HF) in the *RetΔGlut1* retina at 1 month of age which became more numerous in older animals (Figure 6A,B). HF has been correlated to infiltrating microglia and/or macrophages in the outer retina.[56,57] To verify that HF foci corresponded to microglia and/or myeloid cells, retina cryosections were labeled with an antibody to Iba-1 (Figure 6C). We found Iba-1 labeled cells in the outer retina of *RetΔGlut1* but not in control mice. At 1 month of age, these were more likely to be localized to the OPL; by 4 months we noted their infiltration into the sub-retinal space.

To better understand the timing and location of the degenerative changes indicated by SD-OCT, we performed TUNEL assays on retinal sections from *RetΔGlut1* and control mouse eyes at P15 and P30 (Figure 6D). *RetΔGlut1* photoreceptors undergo cell death as early as P15, as numerous TUNEL-positive cells were detected in the ONL but not in the INL or GCL (Figure 6D). We observe similar patterns and the number of TUNEL-positive cells in the ONL of the P30 *RetΔGlut1* retina (data not shown). The ONL-specific TUNEL signal suggests that photoreceptors require GLUT1 for survival, and that cell death occurs during post-natal and adult stages.

Since the glycolytic intermediate glucose-6-phosphate (G6P) is used in the pentose phosphate pathway for the renewal of NADPH, a key electron donor in the cell's antioxidant defense system, loss of GLUT1 in the outer retina would inhibit this system leading to oxidative stress resulting in cell death. To test the hypothesis that elevated oxidative stress contributes to the photoreceptor degeneration observed in *RetΔGlut1* mice, cryosections were stained with avidin, a probe for oxidative DNA damage.[58,59] At

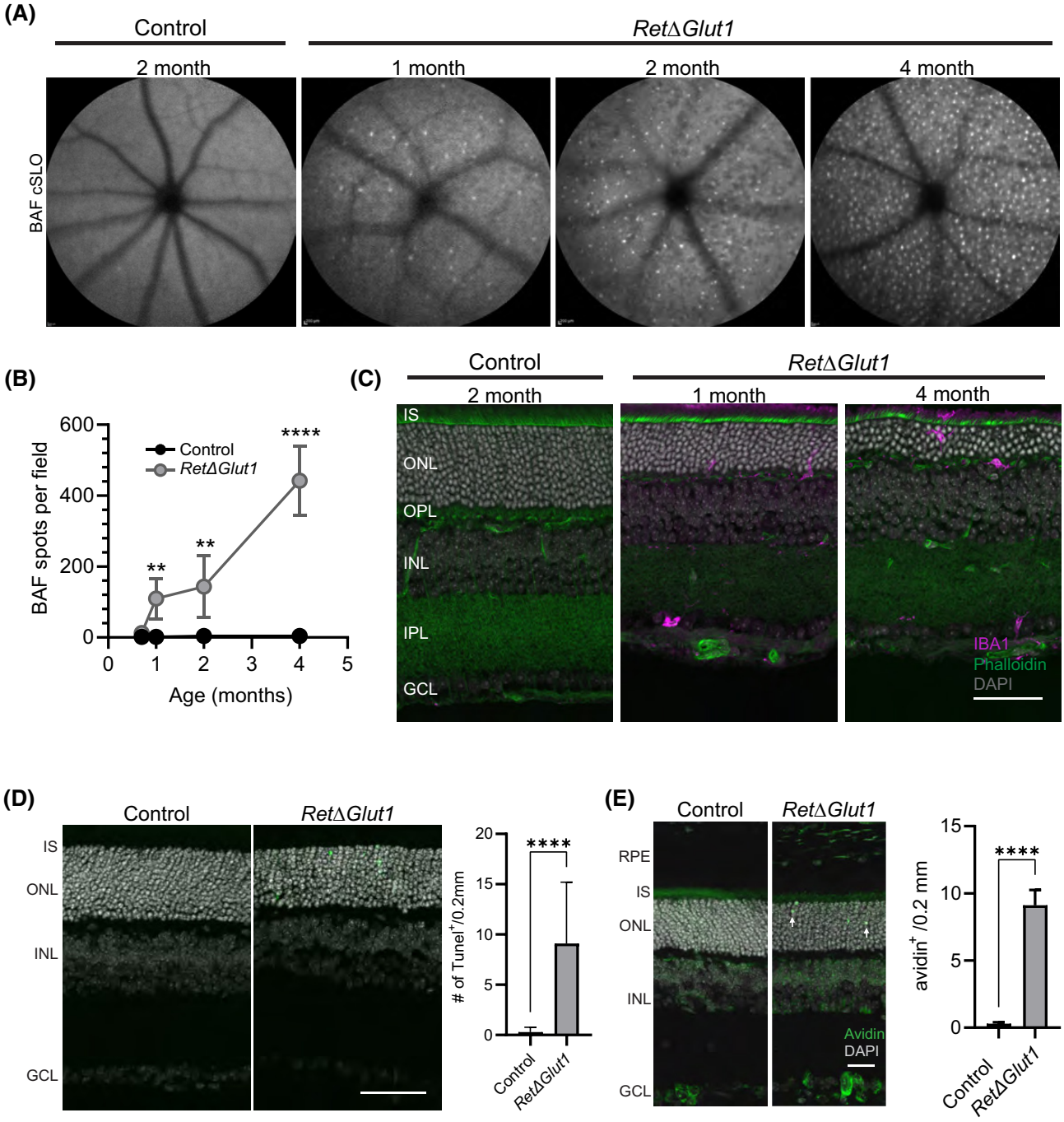

FIGURE 6 Increased inflammation in the outer retina of *RetΔGlut1* mice (A) Representative 55° wide-field BAF-cSLO images obtained from 2-month control and 1-, 2-, and 4-month *RetΔGlut1* mice. (B) The number of BAF-cSLO identified hyperfluorescent foci was quantified at each age in *RetΔGlut1* and control mice. Data points indicate average ± SD for 3–6 mice. (C) Iba-1 immunofluorescence (magenta) in retina cryosections from control, 2 and 4 months *RetΔGlut1* mice counterstained with Phalloidin (green) DAPI (gray). Scale bar indicates 50 μm. IS, inner segments; ONL, outer nuclear layer; OPL, outer plexiform layer, INL, inner nuclear layer; IPL, inner plexiform layer, GCL, ganglion cell layer (D) Left: TUNEL labeling (green) of retina cryosections from P15 control and *RetΔGlut1* mice, counterstained with DAPI (gray). The scale bar indicates 50 μm. Right: quantification of TUNEL per 0.2 mm length retina from immunofluorescent images. Bars indicate the average ± SD for 2 mice. (E) Left: Avidin labeling (green) of retina cryosections from control and *RetΔGlut1* at P15 with DAPI counterstain (gray). The scale bar indicates 25 μm. Right: Quantification of avidin positive cells in oriented fluorescence images within 0.2 mm wide field of view. Bars indicate the average ± SD for 3 mice. GCL, ganglion cell layer; INL, inner nuclear layer; IS, inner segments; ONL, outer nuclear layer; RPE, retinal pigmented epithelium.

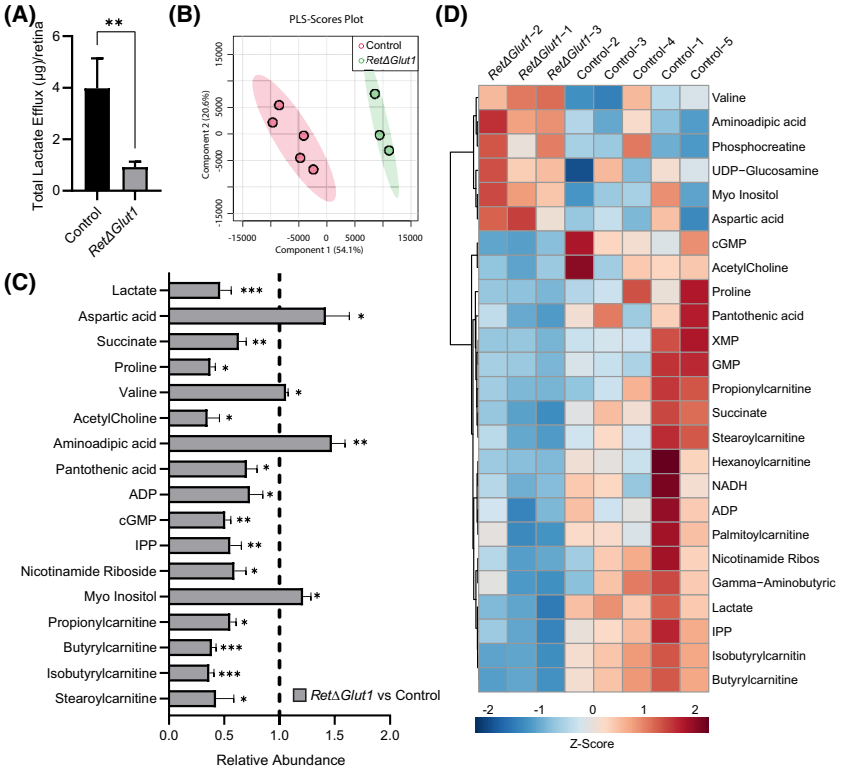

FIGURE 7 *RetΔGlut1* mice have reduced lactate efflux and an altered metabolic profile (A) Lactate efflux from isolated retinas incubated for 1 h in Ringer's with 5 mM glucose from control and *RetΔGlut1* mice. Bars indicate the average ± SEM for 4 retinas. (B) Partial Least-Squares Discriminant Analysis (PLS-DA) of Control and *RetΔGlut1* samples from LC–MS data. Data points indicate results from 5 control and 3 *RetΔGlut1*. (C) Metabolomics analysis of significant metabolites changed in *RetΔGlut1* retina samples. Raw data were normalized to the control average (hashed line), and statistical significance was obtained from *T*-tests after Pareto scaling. Bars indicate the average (± SD) for 3–5 mice (D) Heat map of top 25 metabolites changed based on the statistical significance or fold change between control and *RetΔGlut1* retina samples, after Pareto scaling.

P15 when elevated TUNEL staining was observed, there were numerous avidin-positive cells in the *RetΔGlut1* ONL that were only rarely encountered in control retinas (white arrows indicate representative avidin-positive nuclei, Figure 6E), indicating that reduced glucose uptake elevates oxidative stress leading to photoreceptor degeneration. No differences in avidin staining of INL and GCL were observed between control and *RetΔGlut1* mice, consistent with the lack of TUNEL-positive cells in these retinal cell layers.

3.7 | Retinas lacking GLUT1 have an altered metabolic profile

Studies with isolated retinas demonstrate that large amounts of lactate are released when glucose is present in the media.[60–62] The high rate of aerobic glycolysis has been attributed to photoreceptors despite the fact that *Slc2a1* expression is higher in MGCs (Figure 1A). To investigate the impact of *Slc2a1* deletion on the rate of aerobic glycolysis, lactate efflux was measured from the media after incubation of neural retinas for 1 h with Ringer's buffer supplemented with 5 mM of glucose. Isolated *RetΔGlut1* retinas released fourfold less lactate in comparison to controls (Figure 7A) indicating that retinal aerobic glycolysis depends on glucose uptake via GLUT1.

To understand how restricted glucose uptake affected metabolic pathways in the retina, targeted steady state metabolomics was undertaken with LC MS/MS focusing on amino acids, tricarboxylic acid cycle (TCA) metabolites, nucleotides, and carnitines from 1-month-old control and *RetΔGlut1* neural retinas. A multivariate analysis, Partial Least-Squares Discriminant Analysis (PLS-DA), was used to determine if *RetΔGlut1* neural retinas were different from the controls. Control and *RetΔGlut1* retinas form two distinct clusters indicating an overall difference in their metabolic profiles (Figure 7B). Next, to understand the significant differences between controls and *RetΔGlut1* neural retinas, we performed *t*-tests from normalized LC MS/MS values and identified 17 significantly changed metabolites out of 90 measured metabolites (Figure 7C). A heatmap of the top 25 metabolites was generated based

either on the statistical significance or degree of fold change (Figure 7D).

Lactate levels were lower in *RetΔGlut1* samples, consistent with our efflux measurements and with reduced retinal glycolysis. The TCA cycle intermediate succinate was decreased, while aspartic acid, a derivative from the TCA cycle, had increased abundance. Mitochondrial acyl-carnitines (AC) serve as the precursors for fatty acid oxidation (FAO) that could meet the energetic needs of the neural retina. We found a decreased abundance of propionyl-, isobutyryl-, butyryl-, and stearoyl-carnitine species (Figure 7C,D) in the *RetΔGlut1* mouse suggesting enhanced FAO. Proline levels were significantly decreased (Figure 7C) suggesting an increase in proline catabolism. The metabolic profile of the *RetΔGlut1 retina* is characterized by depletions in AC which are suggestive of increased amino acid catabolism and FAO in the absence of GLUT1 transport activity.

3.8 | Rods depend on glucose uptake through GLUT1 for normal visual function and viability

The impairment of visual function in *RetΔGlut1* mice could result from a lack of glucose uptake into photoreceptor cells directly. Conversely, it could also result secondarily from a lack of glucose transport into MGCs, as they can generate metabolites from glucose to support photoreceptor function.[10,50,63,64] To distinguish these possibilities, we investigated the functional and structural impact of *Slc2a1* deletion in rods by crossing *Glut1*$^{flox/flox}$ mice with transgenic mice having tamoxifen-inducible *Cre* expressed under the control of the rod *Pde6g* promoter (*RodΔGlut1*). To confirm the deletion of GLUT1 from rods, we performed in situ hybridization and immunohistochemistry in control and *RodΔGlut1* retinas 1 month after tamoxifen induction (Figure 8A,B). We noted a loss of signal from the *Slc2a1* RNAscope probe from the ONL and IS layer in the *RodΔGlut1* retinas (Figure 8A). Similarly, a reduction in the signal by anti-GLUT1 immunolabeling was seen in the IS, ONL, and OPL. The remaining GLUT1 staining can be attributed to the MGC apical processes (Figure 8B).

It has been known that GLUT1 protein is highly expressed in the neural retina, however, it was not known how much of the signal was attributed to photoreceptors. To quantify the relative contribution of rods to total retinal GLUT1 levels, western blot analysis for GLUT1 from 1-month-old control, *RetΔGlut1* and *RodΔGlut1* retinas was performed, with vinculin serving as control (Figure 8C). The western blot quantification showed that GLUT1 expression is reduced by ~20% in *RodΔGlut1* mice. The larger GLUT1 reduction seen in the *RetΔGlut1* model, by ~85% of control, indicates that rod photoreceptors account for a modest fraction of total GLUT1 present in the neural retina.

To gain insight into whether glucose directly or indirectly supports rod photoreceptor cells, we measured the structural and functional changes in the retinas of 1-month post-tamoxifen-treated control and *RodΔGlut1* mice. ONL thickness and rod OS length were measured from cryosections that were immunolabeled with RHO and DAPI (Figure 8D). ONL thickness of *RodΔGlut1* was not altered, however, OS length was ~70% of that of controls. ERG a-waves were reduced in *RodΔGlut1* retinas as were ERG b-waves (Figure 8E). In comparison, photopic b-waves reflecting the function of the cone pathway revealed modest changes in amplitude (Figure 8F). We compared peak a-wave and peak scotopic and photopic b-wave amplitudes elicited by 1.4 cd s/m^2 flash stimuli (Figure 8G). The kinetics of the leading edge of the a-wave were comparable to control in both the *RetΔGlut1* and *RodΔGlut1* mice, indicating that rods retained normal phototransduction in the absence of GLUT1 (not shown). Scotopic a-waves were reduced by 40% (233 μV ± 94 vs. 383 μV ± 82, mean ± SD), b-waves were reduced by ~30% (794 μV ± 189 vs. 1180 μV ± 241, mean ± SD) and photopic b-waves were reduced by ~25% (231 μV ± 19 vs. 304 μV ± 58, mean ± SD).

FIGURE 8 Loss of GLUT1 from rods results in impaired OS turnover and reduced ERG amplitude, but impacts are less severe than in *RetΔGlut1* (A) In situ hybridization for *Slc2a1* transcripts (red) in control and *RodΔGlut1*. The scale bar indicates 50 μm. (B) Immunofluorescence for GLUT1 (green) in control and *RodΔGlut1* retinas. The scale bar indicates 50 μm. (C) Western blot analysis of GLUT1 expression in control, *RetΔGlut1*, and *RodΔGlut1* retinas (5 μg/well). Blots are representative of $N = 3$ mice. Quantification of relative expression of GLUT1 in retinas of control, *RetΔGlut1*, and *RodΔGlut1*. The intensity of GLUT1 was normalized to Vinculin. Bars indicate the average (± SD) for 3 mice. (D) Retina cryosections from control and *RodΔGlut1* mice 1-month post-tamoxifen injection immunolabeled for RHO (red) and counterstained with DAPI (blue). The scale bar indicates 25 μm. ONL thickness and OS lengths were estimated with ImageJ. Bars indicate the average (± SD) for 3 mice. (E) Luminance response plots from peak amplitudes of scotopic a-waves and b-waves were recorded from control and *RodΔGlut1* mice 1-month post-tamoxifen injection. Data points indicate average (± SEM) for 7 mice (F) Luminance response plots from photopic b-waves of control and *RodΔGlut1* mice 1-month post-tamoxifen injection. Data points indicate average (± SEM) for 7 mice (G) Maximum amplitudes for scotopic a- and b- waves (S:a-wave, and S:b-wave) and photopic b-wave (P:b-wave) at 1.4 log cd · s/m^2 luminance. Bars indicate the average (± SD) for 7 mice. (H) Left: Western blot analysis of expression of RHO (0.25 μg/well), and ARR1 (0.25 μg/well) in control and *RodΔGlut1* mice 1-month post-tamoxifen injection. Right: Bars indicate the average (± SD) for 5–7 mice.

Our data indicate that glucose uptake into rods is required for rod function and that cones depend on a metabolite derived from glycolysis in rods. Finally, western blot analysis for RHO, and ARR1 revealed that RHO protein levels were reduced to 50% of controls while ARR1 was not changed significantly (Figure 8H).

In both *RetΔGlut1* and *RodΔGlut1* mice, there were changes in OS length and RHO protein expression. However, in contrast to *RetΔGlut1* mice, the ONL thickness of *RodΔGlut1* remained unaltered at 1 month of age while the ONL of *RetΔGlut1* mice was reduced by 20%.

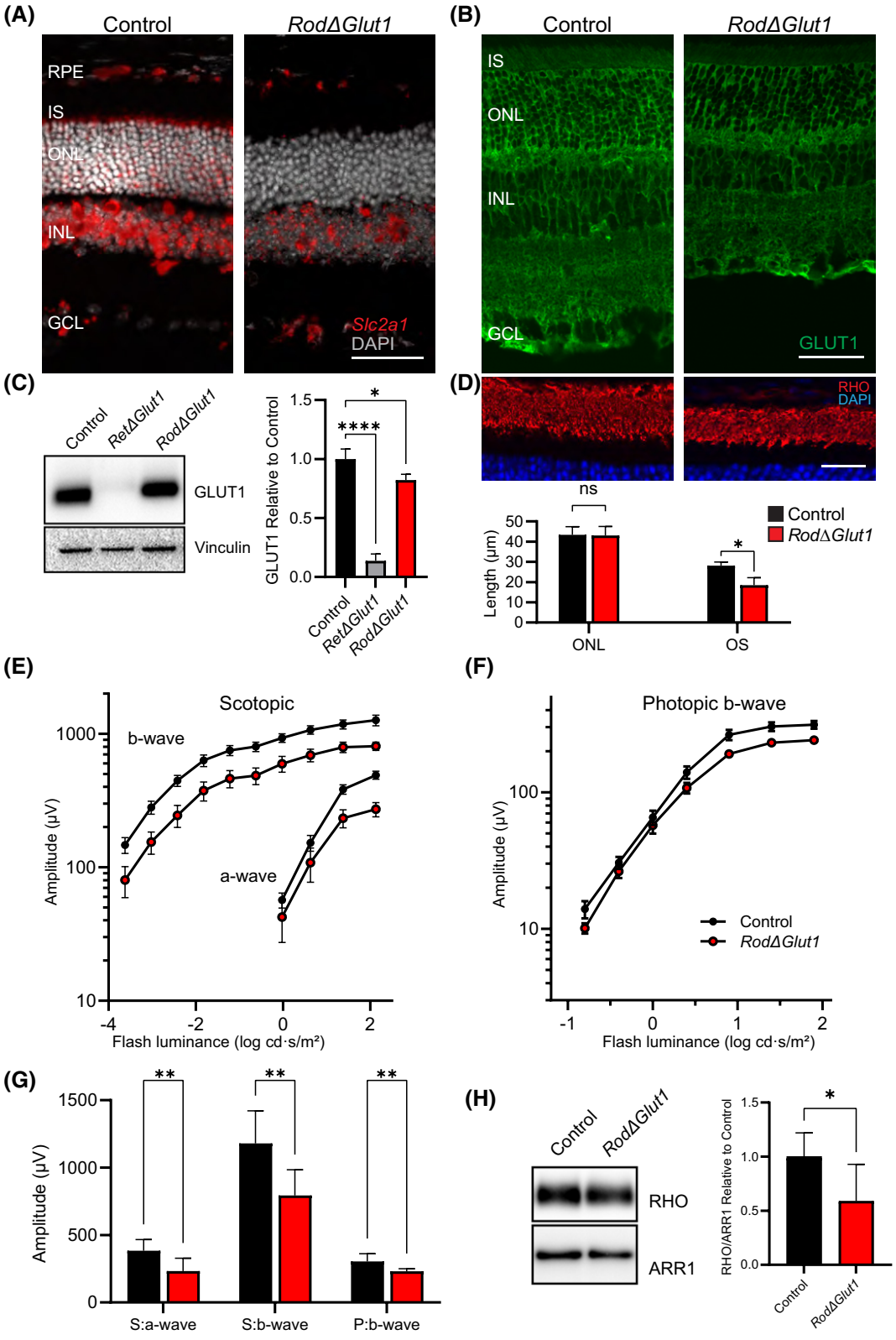

The comparisons of functional and structural parameters in *RodΔGlut1* and *RetΔGlut1* mice indicate that rod photoreceptors require the direct uptake of glucose via GLUT1. Responses of photoreceptors to glucose deprivation were similar in *RodΔGlut1* and *RetΔGlut1* mice, although the magnitude of impairments was greater for *RetΔGlut1* at 1 month. However, the *RodΔGlut1* model was generated by tamoxifen-induced Cre activation at 1 month of age. Since the *Cre* expressed in our *RetΔGlut1* line is not dependent on tamoxifen for activity and is turned on early in development, the timing of Cre-mediated excision and full GLUT1 ablation may differ in the two models. Therefore, we examined the impacts on retinal structure and anatomy with SD-OCT at 4 months post-tamoxifen injection in our *RodΔGlut1* mice and compared this with 4-month-old *RetΔGlut1* mice. (Figure S3A). As shown for *RetΔGlut1* mice (Figure 3A) we observe attenuated reflectivity in B-scans of *RodΔGlut1* mice corresponding to the OLM, the photoreceptor transition zone, and OS tips. ONL thinning is comparable in both *RetΔGlut1* and *Rod ΔGlut1*. cSLO images show numerous BAF foci in *RodΔGlut1* 4 months post-tamoxifen, akin to that of the 4-month-old *RetΔGlut1* (Figure S3B). We quantified the ONL thickness from SD-OCT scans of *RodΔGlut1* and compared this to *RetΔGlut1* and controls (Figure S3C). ONL thickness was reduced by 41% in *RodΔGlut1* at this timepoint, similar to the 45% reduction in *RetΔGlut1* mice. We also quantified the OS layer thickness from B-scans of *RodΔGlut1* mice and observed a 60% decrease in both *RodΔGlut1* and *RetΔGlut1* mice (Figure S3D). We also quantified the number of BAF spots in cSLO images from *RodΔGlut1* and found a similar number of foci compared with *RetΔGlut1* (Figure S3E). Taken together our data argue that glucose uptake in rods is required for OS biosynthesis and viability in a cell-autonomous manner.

To confirm that BAF foci observed in *RodΔGlut1* originate from microglia as was the case for *RetΔGlut1* mice, cryosections of 4-month post-tamoxifen *RodΔGlut1* and 4-month-old *RetΔGlut1* mice were immunolabeled with Iba-1 (Figure S4A). We observed Iba-1 positive cells throughout the photoreceptor layer of both *RetΔGlut1* and *RodΔGlut1* mice, indicating increased microglia infiltration accompanying photoreceptor degeneration in these models. Reactive gliosis is often observed in retinas undergoing photoreceptor degeneration and is readily observed using GFAP immunolabeling. We find elevated GFAP in both *RodΔGlut1* and *RetΔGlut1* retinas (Figure S4B).

4 | DISCUSSION

Glucose is an essential metabolite for the neural retina, where it is used to fuel high rates of glycolysis and mitochondrial respiration.[4,62] Reduced transport of glucose into the outer retina is implicated in photoreceptor loss in animal models of human RP.[3] Therefore, an understanding of the glucose transporters expressed in the neural retina and the impact of glucose deprivation is needed to develop rational treatment strategies to repair nutrient imbalances and prevent photoreceptor cell death. In this study, we determined that *Slc2a1*, encoding for GLUT1, was the primary glucose transporter in the outer retina and used conditional targeting to ablate *Slc2a1* from all retinal neurons and glia (*RetΔGlut1*) or only from rod photoreceptors (*RodΔGlut1*). Pan-retinal deletion of GLUT1 resulted in impairments in opsin biosynthesis and OS renewal in photoreceptors which contributed to rod photoreceptor death. Rod-specific deletion resulted in similar impairments in OS renewal, but rod cell death was not initially observed.

4.1 | GLUT1 is an essential transporter in the outer retina

The *RetΔGlut1* retina appeared normal at P12 but displayed progressive thinning of the ONL at later ages and elevated apoptosis was observed as early as P15. No thinning or TUNEL staining was detected in the INL or GCL at any age. *Slc2a3* encodes GLUT3, a high affinity and high-capacity glucose transporter, which is expressed in tissues having lower interstitial glucose concentration compared with blood, such as the brain.[65] GLUT3 is present in the inner retina[38,39] and in situ, Western blotting and immunofluorescence data showed that photoreceptors do not upregulate *Slc2a3* expression to compensate for deletion of *Slc2a1* (Figure 2D,E). The lack of inner retinal cell loss indicates that glucose uptake via GLUT3 supports the viability of inner retinal cells.

4.2 | Photoreceptors differentiate normally in *RetΔGlut1* mice

In *RetΔGlut1* mice, *Cre* expression is driven by the *Crx* promoter that turns on beginning at E12.5 in photoreceptor progenitors of the outer neuroblast layer.[66,67] However, *Crx* expression is sparse at E12.5 and corresponds to a small population of early-born photoreceptors. *Crx* expression does not peak until P6 when most rods have been born.[66–68] Consistent with this spatiotemporal timing of Crx activity, we observe significant residual expression of GLUT1 at P3. By P10 GLUT1 expression declined and was only encountered in isolated patches within the retina (data not shown). A delay in the complete turnover of residual GLUT1 after *Slc2a1* gene excision may explain

prolonged GLUT1 expression in the early post-natal *RetΔGlut1*.

It is interesting that all *RetΔGlut1* photoreceptors appear to differentiate normally and begin to form an OS. However, overall energy expenditures may be relatively low before eye-opening as rod photoreceptor OS formation is not initiated until ~P10.[46,52] The largest share of ATP consumption in the retina is from ATPase pumps that maintain the ion gradients to enable neuronal signaling.[69] The light responses recorded from photoreceptors of 2-week-old mice are very small, and a fully mature OS structure is not achieved until mice are 3 weeks old.[51,70,71] Thus, lower ATP consumption during neonatal development may allow the diversion of metabolites toward the anabolic requirements of building an OS. In addition, nursing neonates may rely more on alternative fuel sources such as ketones from the mother's milk.[72]

4.3 | Rods and cones depend on GLUT1 activity for outer segment renewal

Though photoreceptors are non-dividing cells, the daily renewal of their OSs imposes a high biosynthetic demand. In this study, we showed that in the *RetΔGlut1* mice, photoreceptor OSs never reach the adult length and *RodΔGlut1* mice have shortened OSs (Figure 5A,B). At P12, rod and cone OS lengths in *RetΔGlut1* mice were not significantly different from controls. By P20, however, OS length lagged in *RetΔGlut1* mice (Figure 3F) and RHO levels were already 50% lower than in controls (Figure 5C).

RHO constitutes ~90% of OS protein and achieving a full-length OS depends on sustaining a high level of RHO synthesis.[47,48,73] In *RetΔGlut1* mice the OS did not increase in length after P20 while control OSs continued to grow to their full adult length (Figure 3F). Based on our observations of normal numbers of RHO positive foci within the *RetΔGlut1* RPE after peak phagocytosis (Figure S2), we can assume that the rate of OS shedding has not been altered. Our data suggest that a decreased rate of opsin synthesis impairs OS renewal by lowering the rate of basal OS replacement. Rod photoreceptors can make a light-responsive OS with <15% of the normal opsin expression, however this low-level opsin expression results in rod death.[73–75] Therefore, the rod cell death observed in the *RetΔGlut1* mouse could be secondary to decreased rhodopsin. By 1 month, ERG amplitudes were greatly reduced in *RetΔGlut1* mice (Figure 3D,E). This reduction reflected ONL thinning (by ~20%) and shortened OSs (by ~50%) and reduced RHO expression.

OS renewal depends on anabolic building blocks (e.g., amino acids, lipid precursors) derived from glucose metabolism. Both the *RetΔGlut1* and *RodΔGlut1* mice phenocopy the defects observed when GLUT1 was knocked out of *RPE*, which resulted in shortened OS and photoreceptor degeneration.[7] Taken together, these findings support the model in which glucose is taken up by the RPE from the choroidal blood supply by GLUT1 at the basal membrane, delivered to the subretinal space by apical RPE GLUT1, and then is transported into rod photoreceptors via GLUT1. Our study demonstrates that glucose is an obligatory carbon source for rod photoreceptor cell OS maintenance and viability.

Impairments in OS formation have been observed in mice with rod-specific ablation of genes encoding glycolytic enzymes such as lactate dehydrogenase A (LDHA), hexokinase 2 (HK2), or pyruvate kinase muscle isozyme 2 (PKM2).[9,11,12,21] When we ablated *Slc2a1* specifically in rods, OS length was reduced by 34% of control, and a-wave amplitudes were comparably reduced. The impaired OS renewal observed in *RodΔGlut1* mice most closely resembled the 20%–50% reduction in OS length observed in the rod-specific HK2 conditional knockout,[12] as opposed to the milder phenotype seen in the conditional knockout of PKM2 in rods.[9] This may not be surprising considering HK is the very first enzyme in glycolysis and that in *RodΔGlut1* photoreceptors we are restricting access in rods to the substrate itself. However, even in HK2 knockout rods, the impact was only seen in aged mice.[11,12] In contrast, photoreceptor OS length was reduced soon after short hairpin RNA was used to ablate PKM2 or LDHA expression.[21] This suggests that with conditional gene targeting strategies, developmental compensatory upregulation of isozymes (e.g., HK1) can partially overcome deficits caused by the gene deletion, whereas this may not occur with overexpression of short hairpin RNAs that interfere post-transcriptionally.

4.4 | Possible influence of glucose availability on rhodopsin transcription

We found a reduced transcription of rhodopsin but not cone opsin, suggesting that biosynthesis of the rod but not cone OS results in part from impaired opsin transcription. A reduction in transcript levels of rod-specific proteins might be expected in 1-month-old *RetΔGlut1* mice, given the observed loss of ONL thickness at this age. However, it is possible that rhodopsin transcription is repressed in response to the altered metabolic state in *RetΔGlut1* mice. For example, Krüppel—like factor 15 (KLF15) represses transcription of both rhodopsin and IRBP by binding to their promoters.[76,77] While KLF15 is normally not expressed in differentiated photoreceptors, it is induced in muscle by prolonged fasting and exercise, where it acts as a transactivator of GLUT4 expression and regulates the expression of mitochondrial Acetyl-CoA synthetase 2.[78–80] Thus, we can speculate that

expression of KLF15, or that of another transcriptional silencer of rhodopsin responsive to nutritional state, could be induced in glucose-depleted rods.

4.5 | Rods but not cones require GLUT1 for survival

RetΔGlut1 mice showed a selective loss of rod photoreceptors despite GLUT1 ablation from both rods and cones. The demise of rods in *RetΔGlut1* mice is accompanied by increased ONL staining for avidin, a marker of oxidatively damaged DNA, suggesting that glucose is required for protection from oxidative stress in rods. In contrast, cone viability was unaffected in *RetΔGlut1* mice at 4 months of age when marked rod degeneration was observed.

While cone function was compromised due to shortened OS (Figure 5B), the degree of cone survival was surprising, since it has been reported that cones require the upregulation of aerobic glycolysis to prolong their survival.[2,3,81] In mouse models, where a genetic mutation causes rod photoreceptor cell death, rods upregulate the secretion of a thioredoxin-like protein (rod-derived cone viability factor, RdCVF) that is thought to bind to cones via Basigin 1, in order to stabilize GLUT1 in the plasma membrane of cones.[2] This mechanism allows continued cone survival in the face of rod degeneration. At late-stage RP, cones lose this trophic support and die. AAV-mediated overexpression of RdCVF is able to rescue cone photoreceptors in late-stage RP.[2] While neither the *RetΔGlut1* nor the *RodΔGlut1* mouse is a model of RP, we observed that during rod degeneration, GLUT1 was not needed to maintain cone survival, suggesting there may be an alternative mechanism of RdCVF-mediated cone survival.

In a non-diseased rod dominant retina, it was proposed that cones may rely more on oxidative phosphorylation than on glycolysis.[6,43] A recent study using the *rd10* mouse showed exogenous lactate was sufficient to promote cone survival when TCA cycle activity was boosted by overexpression of thioredoxin interacting protein (*Txnip)* allele. The rescue was also dependent on LDHB, which catalyzes the conversion of lactate to pyruvate.[82] Cones of *RetΔGlut1* mice have impaired glucose uptake and also face lower overall retinal lactate. There are several possible sources for metabolites supporting cone survival in this unique context. One possibility is that cones receive sufficient lactate (or pyruvate) from microglia, as activated microglia have been shown to upregulate aerobic glycolysis.[83] During retinal degeneration, microglia localized to the ONL and subretinal space may provide cones with lactate and be beneficial to their initial survival. The nature of the metabolic supports for cones in *RetΔGlut1* awaits further study.

4.6 | Targeted metabolomics indicate a shift in substrate utilization in *RetΔGlut1* mice

The *RetΔGlut1* neural retina metabolome showed a reduction in various acylcarnitines (Figure 7), a phenomenon also reported in mice with a retinal or rod-specific knockout of *Mpc1* or *Vldlr*.[5,84] Our metabolomic analysis reflects steady state levels of retina-derived metabolites, so decreases could arise from reduced synthesis or increased utilization. Decreased nicotinamide riboside and pantothenic acid are consistent with an increased reliance on FAO in the retina in the absence of GLUT1 expression. Nicotinamide riboside is a salvageable NAD+ precursor providing a source of additional NAD^+ required for FAO.[85,86] Pantothenic acid is a precursor in the synthesis of CoA, necessary for the activation of acyl groups for FAO. Reduced propionyl- and isobutyryl- carnitines are suggestive of not only enhanced FAO but also increased branched-chain amino acid catabolism.[87,88] Reduced abundance of acylcarnitines, nicotinamide riboside, and pantothenic acid suggest elevated FAO in the *RetΔGlut1*. Alternatively, the lower abundance of acetyl groups (in carnitines and as acetyl-CoA), may highlight lower overall rates of lipid synthesis in the limited glucose supply of *RetΔGlut1* mouse outer retina. Lower phospholipid availability could explain the selective impairment in the synthesis of membrane glycoproteins (photoreceptor opsin) compared with soluble proteins of similar cellular abundance in *RetΔGlut1* mice (ARR1) (Figure 5C).

We also observe elevated aspartate levels in the retinas of *RetΔGlut1* mice, which could result from depleted pyruvate levels and therefore less acetyl-CoA available to enter the TCA. The resultant accumulation of oxaloacetic acid would be expected to result in excess transamination to aspartate, as is the case in the retina-specific MPC1 knockout.[4] Accumulation of aspartate suggests that alternative fuels in the *RetΔGlut1* retina are insufficient to support metabolic needs.

The decreased abundance of proline in the *RetΔGlut1* retina suggests that proline use may be elevated to replenish depleted metabolites, such as pyruvate, in the absence of GLUT1. Proline is a key nutrient for the RPE, where it is catabolized in mitochondria to produce glutamate, α-ketoglutarate, and pyruvate, which are secreted to fuel the retina.[36] Proline is taken up by the retina but at a much slower rate compared with RPE.[36] The activity of the first enzyme in proline catabolism, proline dehydrogenase, is lower in the retina compared with RPE due to repression by high lactate and succinate.[89,90] However, in the *RetΔGlut1* mouse with impaired glycolysis, proline dehydrogenase activity may be de-repressed as was found to be the case in a lung cancer cell line along with increased expression after glucose

deprivation.[91] This shift would be unexpected given the preference of mammalian retinas for aspartate and glutamate as fuel sources under normal conditions.[92] Indeed, proline abundance may be lower due to lower synthesis in the retinas of *RetΔGlut1* mice since it relies on the availability of mitochondrial NADPH produced from NAD+ by NAD kinases, whose activity may be regulated by nutritional status.[93]

Future studies will elucidate the distinct metabolic adaptations in photoreceptors and MGCs to glucose deprivation, and the impacts on the RPE when the normally high lactate efflux from the retina is substantially reduced.

5 | CONCLUSION

In this study, we demonstrated that GLUT1 is the primary glucose transporter in the outer retina, while GLUT3 predominates in the inner retina. When we deleted *Slc2a1* from all retinal neurons and MGC, we observed a selective impact on photoreceptors. In addition to rod cell death, rods and cones had impaired opsin synthesis and shorter OSs. Conditional deletion of *Slc2a1* from only rods also resulted in shorter rod OS. The two models presented here show that glucose uptake into rods is required for opsin synthesis, OS renewal, and viability. Cone survival is less dependent on GLUT1, indicating that cones rely less on glucose and glycolytic intermediates for viability and cell protection. Overall, our findings suggest that glucose deprivation compromises visual function not because of energy deprivation but because of changes in the availability of building blocks required for outer segment renewal.

AUTHOR CONTRIBUTIONS

Lauren L. Daniele, John Y. S. Han, Ivy S. Samuels, all equally contributed to the writing of this manuscript. Nancy J. Philp, Neal S. Peachey, Ivy S. Samuels conceived the project. Nancy J. Philp, Neal S. Peachey, Ivy S. Samuels, John Y. S. Han, and Lauren L. Daniele designed the experiments. Ivy S. Samuels generated the *RetΔGlut1* mice. Neal S. Peachey generated the *RodΔGlut1* mice. Nancy J. Philp, Lauren L. Daniele, John Y. S. Han, Ravikiran Komirisetty, Nikhil Mehta, and Jessica L. McCord performed, and analyzed all biochemical and molecular assays. John Y. S. Han analyzed RNAseq libraries. Ivy S. Samuels, Minzhong Yu and Neal S. Peachey acquired and analyzed ERG data. Yekai Wang and Jianhai Du performed the LC MS/MS, acquired, and analyzed the data. Brent A. Bell and John Y. S. Han performed and acquired SD-OCT and cSLO. John Y. S. Han analyzed SD-OCT data. Lauren L. Daniele analyzed cSLO data. Neal S. Peachey and Kathleen Boesze-Battaglia provided expertise in the interpretation of ERG and metabolomics data.

ACKNOWLEDGMENTS

We would like to thank E. Dale Abel for providing the *GLUT1*$^{flox/flox}$ mice and Stephen Tsang for providing the *Pde6g-CreERT2* mice. We would also like to thank Benjamin Barnhart for his assistance with the analysis of RNAseq libraries.

DISCLOSURES

The authors have no conflicts of interest in connection with this article.

DATA AVAILABILITY STATEMENT

The data that support the findings of this study are available on request from the corresponding author.

ORCID

Lauren L. Daniele https://orcid.org/0000-0002-9397-0342
John Y. S. Han https://orcid.org/0000-0003-4200-5128
Ivy S. Samuels https://orcid.org/0000-0003-1351-031X
Minzhong Yu https://orcid.org/0000-0002-3115-8930
Kathleen Boesze-Battaglia https://orcid.org/0000-0003-0962-0508
Jianhai Du https://orcid.org/0000-0002-2019-8128
Neal S. Peachey https://orcid.org/0000-0002-4419-7226
Nancy J. Philp https://orcid.org/0000-0001-7028-0448

REFERENCES

1. Umino Y, Everhart D, Solessio E, et al. Hypoglycemia leads to age-related loss of vision. *Proc Natl Acad Sci U S A*. 2006;103:19541-19545.
2. Ait-Ali N, Fridlich R, Millet-Puel G, et al. Rod-derived cone viability factor promotes cone survival by stimulating aerobic glycolysis. *Cell*. 2015;161:817-832.
3. Wang W, Lee SJ, Scott PA, et al. Two-step reactivation of dormant cones in retinitis pigmentosa. *Cell Rep*. 2016;15:372-385.
4. Grenell A, Wang Y, Yam M, et al. Loss of MPC1 reprograms retinal metabolism to impair visual function. *Proc Natl Acad Sci U S A*. 2019;116:3530-3535.
5. Wang W, Kini A, Wang Y, et al. Metabolic deregulation of the blood-outer retinal barrier in retinitis pigmentosa. *Cell Rep*. 2019;28:1323-1334.e1324.
6. Petit L, Ma S, Cipi J, et al. Aerobic glycolysis is essential for normal rod function and controls secondary cone death in retinitis pigmentosa. *Cell Rep*. 2018;23:2629-2642.
7. Swarup A, Samuels IS, Bell BA, et al. Modulating GLUT1 expression in retinal pigment epithelium decreases glucose levels in the retina: impact on photoreceptors and Müller glial cells. *Am J Physiol Cell Physiol*. 2019;316:C121-C133.
8. Rajala A, Wang Y, Soni K, Rajala RVS. Pyruvate kinase M2 isoform deletion in cone photoreceptors results in age-related cone degeneration. *Cell Death Dis*. 2018;9:737.

9. Rajala A, Wang Y, Brush RS, et al. Pyruvate kinase M2 regulates photoreceptor structure, function, and viability. *Cell Death Dis*. 2018;9:240.
10. Shen W, Lee SR, Mathai AE, et al. Effect of selectively knocking down key metabolic genes in muller glia on photoreceptor health. *Glia*. 2021;69:1966-1986.
11. Weh E, Lutrzykowska Z, Smith A, et al. Hexokinase 2 is dispensable for photoreceptor development but is required for survival during aging and outer retinal stress. *Cell Death Dis*. 2020;11:422.
12. Zhang R, Shen W, Du J, Gillies MC. Selective knockdown of hexokinase 2 in rods leads to age-related photoreceptor degeneration and retinal metabolic remodeling. *Cell Death Dis*. 2020;11:885.
13. Rajala A, Soni K, Rajala RVS. Metabolic and non-metabolic roles of pyruvate kinase M2 isoform in diabetic retinopathy. *Sci Rep*. 2020;10:7456.
14. Han JYS, Kinoshita J, Bisetto S, et al. Role of monocarboxylate transporters in regulating metabolic homeostasis in the outer retina: insight gained from cell-specific Bsg deletion. *FASEB J*. 2020;34:5401-5419.
15. Zhang Y, Zhang Y, Sun K, Meng Z, Chen L. The SLC transporter in nutrient and metabolic sensing, regulation, and drug development. *J Mol Cell Biol*. 2019;11:1-13.
16. Winkler BS, Starnes CA, Twardy BS, Brault D, Taylor RC. Nuclear magnetic resonance and biochemical measurements of glucose utilization in the cone-dominant ground squirrel retina. *Invest Ophthalmol Vis Sci*. 2008;49:4613-4619.
17. Winkler BS. Glycolytic and oxidative metabolism in relation to retinal function. *J Gen Physiol*. 1981;77:667-692.
18. Ames A 3rd, Li YY. Energy requirements of glutamatergic pathways in rabbit retina. *J Neurosci*. 1992;12:4234-4242.
19. Wang L, Tornquist P, Bill A. Glucose metabolism in pig outer retina in light and darkness. *Acta Physiol Scand*. 1997;160:75-81.
20. Hurley JB. Retina metabolism and metabolism in the pigmented epithelium: a busy intersection. *Annu Rev Vis Sci*. 2021;7:665-692.
21. Chinchore Y, Begaj T, Wu D, Drokhlyansky E, Cepko CL. Glycolytic reliance promotes anabolism in photoreceptors. *eLife*. 2017;6:e25946.
22. Tran DH, Wang ZV. Glucose metabolism in cardiac hypertrophy and heart failure. *J Am Heart Assoc*. 2019;8:e012673.
23. Turco SJ, Pickard JL. Altered G-protein glycosylation in vesicular stomatitis virus-infected glucose-deprived baby hamster kidney cells. *J Biol Chem*. 1982;257:8674-8679.
24. Murray AR, Vuong L, Brobst D, et al. Glycosylation of rhodopsin is necessary for its stability and incorporation into photoreceptor outer segment discs. *Hum Mol Genet*. 2015;24:2709-2723.
25. Young CD, Lewis AS, Rudolph MC, et al. Modulation of glucose transporter 1 (GLUT1) expression levels alters mouse mammary tumor cell growth in vitro and in vivo. *PLoS ONE*. 2011;6:e23205.
26. Holoman NC, Aiello JJ, Trobenter TD, et al. Reduction of Glut1 in the neural retina but not the RPE alleviates polyol accumulation and normalizes early characteristics of diabetic retinopathy. *J Neurosci*. 2021;41:3275-3299.
27. Koch SF, Tsai YT, Duong JK, et al. Halting progressive neurodegeneration in advanced retinitis pigmentosa. *J Clin Invest*. 2015;125:3704-3713.
28. Fadl BR, Brodie SA, Malasky M, et al. An optimized protocol for retina single-cell RNA sequencing. *Mol Vis*. 2020;26:705-717.
29. Stuart T, Butler A, Hoffman P, et al. Comprehensive integration of single-cell data. *Cell*. 2019;177:1888-1902.e1821.
30. Hao Y, Hao S, Andersen-Nissen E, et al. Integrated analysis of multimodal single-cell data. *Cell*. 2021;184:3573-3587.e3529.
31. Peng YR, Shekhar K, Yan W, et al. Molecular classification and comparative taxonomics of foveal and peripheral cells in primate retina. *Cell*. 2019;176:1222-1237.e1222.
32. Wagner E, McCaffery P, Drager UC. Retinoic acid in the formation of the dorsoventral retina and its central projections. *Dev Biol*. 2000;222:460-470.
33. Bell BA, Kaul C, Hollyfield JG. A protective eye shield for prevention of media opacities during small animal ocular imaging. *Exp Eye Res*. 2014;127:280-287.
34. Bell BA, Bonilha VL, Hagstrom SA, Anand-Apte B, Hollyfield JG, Samuels IS. Prolonged ocular exposure leads to retinal lesions in mice. *Exp Eye Res*. 2019;185:107672.
35. Schindelin J, Arganda-Carreras I, Frise E, et al. Fiji: an open-source platform for biological-image analysis. *Nat Methods*. 2012;9:676-682.
36. Yam M, Engel AL, Wang Y, et al. Proline mediates metabolic communication between retinal pigment epithelial cells and the retina. *J Biol Chem*. 2019;294:10278-10289.
37. Pang Z, Chong J, Li S, Xia J. MetaboAnalystR 3.0: toward an optimized workflow for global metabolomics. *Metabolites*. 2020;10:186.
38. Shin BC, Cepeda C, Estrada-Sanchez AM, et al. Neural deletion of glucose transporter isoform 3 creates distinct postnatal and adult neurobehavioral phenotypes. *J Neurosci*. 2018;38:9579-9599.
39. Watanabe T, Nagamatsu S, Matsushima S, Kirino T, Uchimura H. Colocalization of GLUT3 and choline acetyltransferase immunoreactivity in the rat retina. *Biochem Biophys Res Commun*. 1999;256:505-511.
40. Samson M, Emerson MM, Cepko CL. Robust marking of photoreceptor cells and pinealocytes with several reporters under control of the Crx gene. *Dev Dyn*. 2009;238:3218-3225.
41. Gospe SM 3rd, Baker SA, Arshavsky VY. Facilitative glucose transporter Glut1 is actively excluded from rod outer segments. *J Cell Sci*. 2010;123:3639-3644.
42. Kanow MA, Giarmarco MM, Jankowski CS, et al. Biochemical adaptations of the retina and retinal pigment epithelium support a metabolic ecosystem in the vertebrate eye. *eLife*. 2017;6:e28899.
43. He J, Yamamoto M, Sumiyama K, et al. Two-photon AMPK and ATP imaging reveals the bias between rods and cones in glycolysis utility. *FASEB J*. 2021;35:e21880.
44. Daum JM, Keles Ö, Holwerda SJ, et al. The formation of the light-sensing compartment of cone photoreceptors coincides with a transcriptional switch. *eLife*. 2017;6:e31437.
45. Salinas RY, Pearring JN, Ding JD, Spencer WJ, Hao Y, Arshavsky VY. Photoreceptor discs form through peripherin-dependent suppression of ciliary ectosome release. *J Cell Biol*. 2017;216:1489-1499.
46. Obata S, Usukura J. Morphogenesis of the photoreceptor outer segment during postnatal development in the mouse (BALB/c) retina. *Cell Tissue Res*. 1992;269:39-48.
47. Lem J, Krasnoperova NV, Calvert PD, et al. Morphological, physiological, and biochemical changes in rhodopsin knockout mice. *Proc Natl Acad Sci U S A*. 1999;96:736-741.

48. Humphries MM, Rancourt D, Farrar GJ, et al. Retinopathy induced in mice by targeted disruption of the rhodopsin gene. *Nat Genet*. 1997;15:216-219.
49. Daniele LL, Insinna C, Chance R, Wang J, Nikonov SS, Pugh EN Jr. A mouse M-opsin monochromat: retinal cone photoreceptors have increased M-opsin expression when S-opsin is knocked out. *Vision Res*. 2011;51:447-458.
50. Viegas FO, Neuhauss SCF. A metabolic landscape for maintaining retina integrity and function. *Front Mol Neurosci*. 2021;14:656000.
51. Carter-Dawson L, Alvarez RA, Fong SL, Liou GI, Sperling HG, Bridges CD. Rhodopsin, 11-cis vitamin a, and interstitial retinol-binding protein (IRBP) during retinal development in normal and rd mutant mice. *Dev Biol*. 1986;116:431-438.
52. Duncan JL, LaVail MM, Yasumura D, et al. An RCS-like retinal dystrophy phenotype in mer knockout mice. *Invest Ophthalmol Vis Sci*. 2003;44:826-838.
53. Nandrot EF, Kim Y, Brodie SE, Huang X, Sheppard D, Finnemann SC. Loss of synchronized retinal phagocytosis and age-related blindness in mice lacking alphavbeta5 integrin. *J Exp Med*. 2004;200:1539-1545.
54. Yu C, Roubeix C, Sennlaub F, Saban DR. Microglia versus monocytes: distinct roles in degenerative diseases of the retina. *Trends Neurosci*. 2020;43:433-449.
55. Guo M, Schwartz TD, Dunaief JL, Cui QN. Myeloid cells in retinal and brain degeneration. *FEBS J*. 2021;289:2337-2361.
56. Flynn E, Ueda K, Auran E, Sullivan JM, Sparrow JR. Fundus autofluorescence and photoreceptor cell rosettes in mouse models. *Invest Ophthalmol Vis Sci*. 2014;55:5643-5652.
57. Bell BA, Kaul C, Bonilha VL, Rayborn ME, Shadrach K, Hollyfield JG. The BALB/c mouse: effect of standard vivarium lighting on retinal pathology during aging. *Exp Eye Res*. 2015;135:192-205.
58. Sanz MM, Johnson LE, Ahuja S, Ekstrom PA, Romero J, van Veen T. Significant photoreceptor rescue by treatment with a combination of antioxidants in an animal model for retinal degeneration. *Neuroscience*. 2007;145:1120-1129.
59. Trachsel-Moncho L, Benlloch-Navarro S, Fernández-Carbonell Á, et al. Oxidative stress and autophagy-related changes during retinal degeneration and development. *Cell Death Dis*. 2018;9:812.
60. Du J, Cleghorn W, Contreras L, et al. Cytosolic reducing power preserves glutamate in retina. *Proc Natl Acad Sci U S A*. 2013;110:18501-18506.
61. Hurley JB, Lindsay KJ, Du J. Glucose, lactate, and shuttling of metabolites in vertebrate retinas. *J Neurosci Res*. 2015;93:1079-1092.
62. Du J, Rountree A, Cleghorn WM, et al. Phototransduction influences metabolic flux and nucleotide metabolism in mouse retina. *J Biol Chem*. 2016;291:4698-4710.
63. Poitry-Yamate CL, Poitry S, Tsacopoulos M. Lactate released by Müller glial cells is metabolized by photoreceptors from mammalian retina. *J Neurosci*. 1995;15:5179-5191.
64. Winkler BS, Arnold MJ, Brassell MA, Puro DG. Energy metabolism in human retinal Müller cells. *Invest Ophthalmol Vis Sci*. 2000;41:3183-3190.
65. Gould GW, Thomas HM, Jess TJ, Bell GI. Expression of human glucose transporters in xenopus oocytes: kinetic characterization and substrate specificities of the erythrocyte, liver, and brain isoforms. *Biochemistry*. 1991;30:5139-5145.
66. Furukawa T, Morrow EM, Cepko CL. Crx, a novel otx-like homeobox gene, shows photoreceptor-specific expression and regulates photoreceptor differentiation. *Cell*. 1997;91:531-541.
67. Montana CL, Lawrence KA, Williams NL, et al. Transcriptional regulation of neural retina leucine zipper (Nrl), a photoreceptor cell fate determinant. *J Biol Chem*. 2011;286:36921-36931.
68. Nishida A, Furukawa A, Koike C, et al. Otx2 homeobox gene controls retinal photoreceptor cell fate and pineal gland development. *Nat Neurosci*. 2003;6:1255-1263.
69. Okawa H, Sampath AP, Laughlin SB, Fain GL. ATP consumption by mammalian rod photoreceptors in darkness and in light. *Curr Biol*. 2008;18:1917-1921.
70. Bakall B, Marmorstein LY, Hoppe G, Peachey NS, Wadelius C, Marmorstein AD. Expression and localization of bestrophin during normal mouse development. *Invest Ophthalmol Vis Sci*. 2003;44:3622-3628.
71. Bonezzi PJ, Stabio ME, Renna JM. The development of mid-wavelength photoresponsivity in the mouse retina. *Curr Eye Res*. 2018;43:666-673.
72. Cunnane SC, Trushina E, Morland C, et al. Brain energy rescue: an emerging therapeutic concept for neurodegenerative disorders of ageing. *Nat Rev Drug Discov*. 2020;19:609-633.
73. Palfi A, Millington-Ward S, Chadderton N, et al. Adeno-associated virus-mediated rhodopsin replacement provides therapeutic benefit in mice with a targeted disruption of the rhodopsin gene. *Hum Gene Ther*. 2010;21:311-323.
74. Sakurai K, Onishi A, Imai H, et al. Physiological properties of rod photoreceptor cells in green-sensitive cone pigment knock-in mice. *J Gen Physiol*. 2007;130:21-40.
75. Shi G, Yau KW, Chen J, Kefalov VJ. Signaling properties of a short-wave cone visual pigment and its role in phototransduction. *J Neurosci*. 2007;27:10084-10093.
76. Otteson DC, Liu Y, Lai H, et al. Kruppel-like factor 15, a zinc-finger transcriptional regulator, represses the rhodopsin and interphotoreceptor retinoid-binding protein promoters. *Invest Ophthalmol Vis Sci*. 2004;45:2522-2530.
77. Botta S, de Prisco N, Marrocco E, et al. Targeting and silencing of rhodopsin by ectopic expression of the transcription factor KLF15. *JCI Insight*. 2017;2:e96560.
78. Yamamoto J, Ikeda Y, Iguchi H, et al. A Kruppel-like factor KLF15 contributes fasting-induced transcriptional activation of mitochondrial acetyl-CoA synthetase gene AceCS2. *J Biol Chem*. 2004;279:16954-16962.
79. Hsieh PN, Fan L, Sweet DR, Jain MK. The Kruppel-like factors and control of energy homeostasis. *Endocr Rev*. 2019;40:137-152.
80. Gray S, Feinberg MW, Hull S, et al. The Kruppel-like factor KLF15 regulates the insulin-sensitive glucose transporter GLUT4. *J Biol Chem*. 2002;277:34322-34328.
81. Punzo C, Kornacker K, Cepko CL. Stimulation of the insulin/mTOR pathway delays cone death in a mouse model of retinitis pigmentosa. *Nat Neurosci*. 2009;12:44-52.
82. Xue Y, Wang SK, Rana P, et al. AAV-Txnip prolongs cone survival and vision in mouse models of retinitis pigmentosa. *eLife*. 2021;10:e66240.
83. Wang L, Pavlou S, Du X, Bhuckory M, Xu H, Chen M. Glucose transporter 1 critically controls microglial activation through facilitating glycolysis. *Mol Neurodegener*. 2019;14:2.
84. Joyal JS, Sun Y, Gantner ML, et al. Retinal lipid and glucose metabolism dictates angiogenesis through the lipid sensor Ffar1. *Nat Med*. 2016;22:439-445.

85. Elhassan YS, Kluckova K, Fletcher RS, et al. Nicotinamide riboside augments the aged human skeletal muscle NAD(+) metabolome and induces transcriptomic and anti-inflammatory signatures. *Cell Rep*. 2019;28:1717-1728.e1716.
86. Mehmel M, Jovanovic N, Spitz U. Nicotinamide riboside-the current state of research and therapeutic uses. *Nutrients*. 2020;12:1616.
87. Newgard CB, An J, Bain JR, et al. A branched-chain amino acid-related metabolic signature that differentiates obese and lean humans and contributes to insulin resistance. *Cell Metab*. 2009;9:311-326.
88. McCann MR, George De la Rosa MV, Rosania GR, Stringer KA. L-carnitine and acylcarnitines: mitochondrial biomarkers for precision medicine. *Metabolites*. 2021;11:51.
89. Kowaloff EM, Phang JM, Granger AS, Downing SJ. Regulation of proline oxidase activity by lactate. *Proc Natl Acad Sci U S A*. 1977;74:5368-5371.
90. Hancock CN, Liu W, Alvord WG, Phang JM. Co-regulation of mitochondrial respiration by proline dehydrogenase/oxidase and succinate. *Amino Acids*. 2016;48:859-872.
91. Pandhare J, Donald SP, Cooper SK, Phang JM. Regulation and function of proline oxidase under nutrient stress. *J Cell Biochem*. 2009;107:759-768.
92. Li B, Zhang T, Liu W, et al. Metabolic features of mouse and human retinas: rods versus cones, macula versus periphery, retina versus RPE. *iScience*. 2020;23:101672.
93. Hoxhaj G, Ben-Sahra I, Lockwood SE, et al. Direct stimulation of NADP(+) synthesis through Akt-mediated phosphorylation of NAD kinase. *Science*. 2019;363:1088-1092.

SUPPORTING INFORMATION

Additional supporting information can be found online in the Supporting Information section at the end of this article.

How to cite this article: Daniele LL, Han JYS, Samuels IS, et al. Glucose uptake by GLUT1 in photoreceptors is essential for outer segment renewal and rod photoreceptor survival. *The FASEB Journal*. 2022;36:e22428. doi:10.1096/fj.202200369R